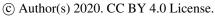SOIL
Discussions
Open Access
EGU

# Iron and aluminum association with microbially processed organic matter via meso-density aggregate formation across soils: organo-metallic glue hypothesis

5   Rota Wagai[1], Masako Kajiura[1], Maki Asano[2]

[1]National Agriculture and Food Research Organization, Institute for Agro-Environmental Sciences. 3-1-3 Kan-nondai, Tsukuba, Ibaraki, 305-8604, Japan
[2]Faculty of Life and Environmental Sciences, University of Tsukuba, 1-1-1 Tennodai, Tsukuba, Ibaraki 305-8572, Japan

*Correspondence to*: Rota Wagai (rota@affrc.go.jp)

10   **Abstract.** Global significance of iron (Fe) and aluminum (Al) for the storage of organic matter (OM) in soils and surface sediments is increasingly recognized. Yet specific metal phases involved or the mechanism behind metal-OM correlations frequently shown across soils remain unclear. We identified density fraction locations of major metal phases and OM using 23 soil samples from 5 climate zones and 5 soil orders (Andisols, Spodosols, Inceptisols, Mollisols, Ultisols), including several subsurface horizons and both natural and managed soils. Each soil was separated to 4 to 7 density fractions using sodium

15   polytungstate with mechanical shaking, followed by the sequential extraction of each fraction with pyrophosphate (PP), acid oxalate (OX), and finally with dithionite-citrate (DC) to estimate pedogenic metal phases of different solubility and crystallinity. The extractable Fe and Al concentrations (per fraction) generally showed unique unimodal distribution along particle density gradient for each soil and each extractable metal phase. Across the studied soils, the maximum metal concentrations were always at meso-density range (1.8-2.4 g cm$^{-3}$) within which PP-extractable metals peaked at 0.3-0.4 g cm$^{-}$

20   $^3$ lower density range relative to OX- and DC-extractable metals. Meso-density fractions, consisted largely of microaggregates based on SEM observation, accounted for on average 56-70% of total extractable metals and OM present in these soils. The OM in meso-density fractions appeared microbially processed from the original plant material. The amounts of PP- and OX-extractable metals correlated positively with co-dissolved C among the soils and, to some extent, across the density fractions within each soil. These results led to a hypothesis which involves two distinct levels of organo-metal interaction – the formation

25   of OM-rich, mixed metal phases having relatively fixed OM:metal stoichiometry and subsequent development of meso-density microaggregates via "gluing" properties of these organo-metallic phases by incorporating other organic and mineral particles such as phyllosilicate clays. Given that stable OM is mainly located in meso-density fractions, soil's capacity to protect OM may be controlled by the balance of following three processes: (i) microbial processing of plant-derived OM, (ii) dissolution of metals, and (iii) the synthesis of organo-metallic phases and their association with clays to form meso-density

30   microaggregates. The current hypothesis may help to fill the gap between well-studied molecular scales interaction (e.g., OM adsorption on mineral surface, coprecipitation) and larger-scale processes such as aggregation, C accrual, and pedogenesis.

# 1 Introduction

Organic matter (OM) stored in soil plays a fundamental role in ecosystem functioning through the storage of carbon (C)

35  and nutrients, improvement of aeration and water-holding capacity, and thus plant productivity and biogeochemical cycling. Changes in soil OM have a significant impact on future climate as soil represents the largest terrestrial C pool. The storage capacity and stability of soil OM are particularly important questions for our efforts to limit global warming (Smith, 2016). Soil OM stability is strongly controlled by its association with soil mineral via chemical interaction and physical aggregation (Lehmann and Kleber, 2015; Sollins et al., 1996). The mineral parameters often used to estimate soil's protective capacity are

40  clay content (<2 μm) or clay plus silt content (<20 μm) of soils as they often correlate with soil OM contents and these small-sized minerals tend to have high surface area to adsorb OM (Six et al., 2002 and the references therein). Commonly-used mathematical models to predict soil C changes use these parameters to slow down OM turnover and to increase its storage (Coleman and Jenkinson, 1996; Parton et al., 1987; Wieder et al., 2015).

On the other hand, global significance of iron (Fe) and aluminum (Al) on OM storage in soil and surface sediments has

45  been increasingly recognized. Using 5500 pedons around the world, Rasmussen et al., 2018) showed stronger control of organic C storage in non-arid soils by oxalate extractable metal content than by clay content. Important linkage among climate (esp. water balance), dissolved organic C production, and its stabilization by these metal phases has been shown on a continental scale (Kramer and Chadwick, 2018). Surface marine sediments also store significant amounts of Fe-bound C (Lalonde et al., 2012). Iron and aluminum, the third and fourth most abundant elements on the earth crust, are in fact highly reactive with OM

50  once released via chemical weathering. These pedogenic metals can be present in monomeric form by chelating with organic ligands or in polymeric form as polynuclear complexes and as secondary minerals. The latter includes Fe and Al oxides, hydroxides, and oxyhydroxides (collectively called metal oxides, hereafter) as well as short-range-order aluminosilicates (allophane, imogolite, and proto-imogolite) that have high sorptive capacity for OM due to their small size (down to several nm) and high surface density of hydroxyl group (Fuji et al., 2019; Kaiser and Guggenberger, 2003; Kleber et al., 2014). In

55  addition, soluble complexes of Fe and Al with organic ligands can be precipitated especially in acidic, OM-rich environments such as volcanic and podzolic soils (Lundström et al., 2000; Percival et al., 2000; Takahashi and Dahlgren, 2016).

Incorporating such metal control into soil C models is still a challenge because the mechanisms by which pedogenic metals control OM storage and stabilization remain elusive. This is partly because current understanding relies largely on OM-metal correlations where the metal concentration often co-varies with other soil properties. The reactive metal contents often

60  positively correlate with other mineralogical parameters that are considered to contribute to OM storage such as clay content and soil specific surface area (e.g., Kaiser and Guggenberger, 2003; Mayer and Xing, 2001). In the long-term pedogenesis (240-4,100 kys) under temperate or tropical moist climate regime, radiocarbon-based soil C stability was positively correlated with extractable metal contents in two chronosequence studies (Masiello et al., 2004; Torn et al., 1997) but not in another study

under wetter climate where only soil specific surface area and halloysite content showed significant correlation (Lawrence et

65 al., 2015). Short-range-order minerals and Fe oxides can also promote aggregation (Churchman and Tate, 1986; Oades and Waters, 1991; Shang and Tiessen, 1998) which indirectly enhances OM stability (Balesdent et al., 2000; Totsche et al., 2017) without necessarily showing proportionality to metal concentrations.

To untangle co-varying factors, Wagai and Mayer (2007) assessed Fe oxide contribution on C storage by quantifying the C released during the reductive Fe oxide dissolution with dithionite for soils covering eight soil orders. After correcting for

70 the OC release due to salt and extractive pH effects, the study conservatively estimated that 2-25% (up to 60% for a highly-weathered, Fe-rich soil) of total soil OM was Fe-bound and the C:Fe ratio of the extracts suggested greater contribution of precipitated organo-metal complexes than simple adsorptive association in lower pH soils. Subsequent dithionite-based studies confirmed that less than half (typically less than a quarter) of total OM were associated with Fe in a range of soils and sediments (Coward et al., 2018; Coward et al., 2017; Lalonde et al., 2012; Zhao et al., 2016). Wagai et al. (2013) further examined the

75 potential contribution of other metal phases such as short-range-order minerals, organo-metal complexes, and their coprecipitates using other extractants and showed that, even as liberal estimates, 5-60% of total OM in a range of acidic to near neutral soils (higher percentages for volcanic soils and spodic horizons) could be explained by direct association with Fe and Al phases. The limited extractability of OM with these metal phases implied the potentially critical role of physical protection via ternary associations of OM, metals, and clay (Wagai and Mayer, 2007). More recent studies showed that a

80 portion of soil Fe phases in soil can be protected from reductive dissolution (dithionite extraction) due presumably to physical protection within microaggregates or co-precipitation with short-range-order aluminosilicates (Coward et al., 2018; Suda and Makino, 2016; Filimonova et al., 2016), suggesting both the limitation of single extraction approach and the importance of aggregation/precipitation reactions. On the other hand, experimental studies revealed specific factors and underlying mechanisms behind OM-metal interaction via adsorption, complexation, and co-precipitation using pure metal phases under

85 well-defined laboratory conditions (Chen et al., 2014; Mikutta et al., 2011; Nierop et al., 2002; Schneider et al., 2010; Tamrat et al., 2019; Kaiser, 2003). However, a large knowledge gap still remains between the laboratory studies and field-based studies (see a review by Kleber et al., 2015).

Critical to filling this gap is to identify factors controlling the distribution and localization of different pedogenic metal phases in soil system because different modes of organo-metal association likely take place at specific local environments. At

90 larger spatial scales, mobilization and accumulation of pedogenic metal phases and their interaction with OM over time and along soil profile depth have been well-recognized (e.g., Kramer et al., 2012; Lawrence et al., 2015). At micro- to nano-meter scales, on the other hand, advanced imaging techniques revealed co-localization of OM and pedogenic Fe and Al in natural soils (Asano et al., 2018; Garcia Arredondo et al., 2019; Inagaki et al., 2020; Wan et al., 2007), although up-scaling of these information remains as a major challenge. At horizon or bulk soil scales, physical fractionation studies have indicated the

95 presence – but not the spatial arrangement – of multiple OM pools of varying turnover rate and degree of mineral associations (Christensen, 2001; von Lützow et al., 2007).

Density provides a useful fractionation approach to assess the localization of pedogenic Fe and Al phases because many biogeochemical characteristics of soil particles are closely related to their density (Christensen, 2001; Sollins et al., 2009; Turchenek and Oades, 1979; von Lützow et al., 2007). The density of soil particles is primarily controlled by the relative

100 amounts of the two major components, OM and mineral. The average density of OM present in soil is typically around 1.4 g cm$^{-3}$ but can range between 1.1-1.9 g cm$^{-3}$ across soils and sediments (Mayer et al., 2004). The minerals typically found in soils such as aluminosilicate clays have the density of >2.4 g cm$^{-3}$ including short-range-order allophane and imogolite (2.75 and 2.70 g cm$^{-3}$, Wada, 2018) with minor exceptions such as phytoliths (2.1-2.15 g cm$^{-3}$, Drees et al., 1989). Among metal oxides, Fe oxides have much higher densities (3.8-5.3 g cm$^{-3}$, Cornell and Schwertmann, 2003) compared with Al oxides such

105 as gibbsite (2.4 g cm$^{-3}$, Anthony et al., 1997). Pedogenic metals can remain as distinct phases, or they can associate with OM or other minerals. From the perspective of OM, both pedogenic metals and other minerals will be found in a high-density fraction (>2.4 g cm$^{-3}$) unless they associate with OM. While OM binding lowers the density of Fe and Al phases in laboratory (Kaiser and Guggenberger, 2007), its extent under various pedogenic environments is virtually unstudied.

We hypothesize that most pedogenic metals are found in <2.4 g cm$^{-3}$ density fractions regardless of soil type due to their

110 high reactivity with OM. Because of the higher density and redox sensitivity, pedogenic Fe may concentrate in different density phases from pedogenic Al for any given soils, assuming that organo-Fe and organo-Al associations take place independently. Alternatively, if the metal dissolution and subsequent interaction with OM are regulated by the same environmental factors, their distribution along the particle density gradient would be similar. Furthermore, if submicron-sized, OM-rich metal phases act as binding agent as suggested for a volcanic soil based on STXM, NEXAFS, and EM (Asano and Wagai, 2014; Asano et

115 al., 2018), they may preferentially bind with other fine-sized minerals (e.g., clays) to form the ternary associations previously postulated (Wagai and Mayer, 2007). These ideas were tested by fractionating soil particles into 4 to 7 density classes after a mild level of dispersion (mechanical shaking in solution) and by quantifying the amounts of Fe and Al phases by selective dissolution techniques that target different metal phases (pyrophosphate, acid oxalate, and dithionite-citrate extractions in sequence) using 23 soil samples from 11 sites spanning 5 climate zones, 5 soil orders (Andisols, Spodosols, Inceptisols,

120 Mollisols, Ultisols), and including several subsurface horizons and both natural and managed (upland and paddy) soils.

Terminology: We use the term "complex" to refer to aqueous organo-metal complexes and their precipitates, and avoid its use to describe broader associations such as organo-clay and organo-mineral complex. Various types of OM-metal association are discussed by grouping into three general mechanisms (adsorption, complexation, and aggregation) while recognizing that organo-metal complexes in soil are mainly coprecipitated with other metal phases and particles. The term

125 "particle" is used in a broad sense to include aggregates as well as single organic or mineral particles.

## 2 Methods

### 2.1 Soil sample source

Soil sample set consisted of four groups: allophanic Andisol, non-allophanic Andisol, spodic, and crystalline mineralogy
130    group (n=23, Table 1), including both natural and cultivated soils from six climate zones with a wide range of mean annual
temperature (5-24 $^{\circ}$C) and precipitation (221-2392 mm yr$^{-1}$). Carbon refers to organic C in this study as no carbonate was
found in these soils. Data from the five Andisol samples (A-1 to A-5) have been reported previously (Wagai et al., 2018). All
samples were air-dried and 2-mm sieved prior to density fractionation and chemical analyses. Air-drying did not significantly
change OM and metal distribution across density, showing no irreversible aggregation by air-drying for an allophanic Andisol
135    (Wagai et al., 2015) and presumably for the other soils.

### 2.2 Physical fractionation by density

We sequentially separated each soil into 4 up to 7 fractions based on particle density using sodium polytungstate (SPT-0
grade, Sometsu, Germany) to make liquids of various densities. We employed mechanical shaking to disrupt less-stable
aggregates following previous studies (Crow et al., 2014; Sollins et al., 2009; Wagai et al., 2018). Density fractions isolated
140    were rinsed with deionized water to desalt until conductivity of final rinse water (50 mL) was <50 µS cm$^{-1}$. The lowest-density
fractions (<1.6 g cm$^{-3}$) were oven-dried at 80 $^{\circ}$C and the other density fractions were freeze-dried for further analyses.

### 2.3 Extraction of metal phases

Bulk and density-fractionated samples were sequentially extracted by sodium pyrophosphate (PP) followed by acid
145    oxalate in dark (OX) and then by dithionite-citrate (DC) following (Wagai et al., 2018). First, initial PP extraction was
conducted at the soil:solution ratio of 100mg:10mL with 0.1 M sodium pyrophosphate (pH=10), and then shaken at 120 rpm
for 16h. After high-speed centrifugation (29,000 g, 45 min), an aliquot of the extract was immediately taken for dissolved C,
N, and metal analyses. Second, the residue after discarding the remaining supernatant was re-suspended and extracted with 10
mL of 0.2 M acidified sodium oxalate solution (pH=3.0), shaken at 120 rpm for 4 h in the dark. The conventional acid oxalate
150    method (Loeppert and Inskeep, 1996) was modified by replacing ammonium oxalate with sodium oxalate to allow the direct
quantification of co-dissolved N while achieving the same extraction efficiency of Fe, Al, and Si (Wagai et al., 2013). After
the high-speed centrifugation, an aliquot of the extract was immediately diluted for metal and N analyses to avoid precipitation.
Third, 0.1 g of sodium dithionite was added to the remaining residue and mixed with 10 mL of 22% (by wt) sodium citrate.
The mixture was shaken for 16 h and centrifuged under the same condition as above. All extractions were done at room
155    temperature (20-22 $^{\circ}$C). We did not filter the supernatants after the high-speed centrifugation of PP extracts as our pilot test
showed no systematic decrease in dissolved organic C and metals by vacuum filtration using 0.025 ☐m pore-sized membrane

(Millipore, VSWP, Bedford, MA, USA). Similarly, no filtration was done for OX and DC extracts after the high-speed centrifugation.

## 2.4 Chemical analyses

160    The concentrations of Fe, Al, Si, and Mn in the extracts of PP, OX, and DC were analyzed by inductively coupled plasma-optical emission spectroscopy (Vista-Pro, Agilent, CA, USA). The metal analyses were done for all fractions. The only exception is the lowest-density fraction from three soil samples (A-5, N-4, C-2) where low mass recovery prevented the extractions. Analytical errors associated with our density fractionation were sufficiently low for C, N, and the extractable metals (<12%, Wagai et al., 2015) to allow testing of our hypothesis. When assessing the role of extractable metal as a whole,
165    we summed weight-based concentrations of Al and Fe as "Al + 0.5Fe" to approximately normalize the atomic mass difference between Al and Fe for graphing and statistical purposes.

Co-dissolved organic C and N by PP extraction and the N by OX extraction were quantified by TOC analyzer (Shimadzu TOC-V/TNM1, Kyoto, Japan). Dissolved organic C (DOC) was measured as non-purgeable organic C after acidification and C-free air purging. Total dissolved N was measured by a chemiluminescence accessory. This method, including the caveats
170    on this technique, was discussed elsewhere (Wagai et al., 2013). Because quantifying the soil C in an oxalate extract is not possible, we estimated the C associated with OX-extractable mineral phases ($DOC_{OX}$) by multiplying total dissolved N concentration in OX extract by the C:N for each density fraction. This estimation assumes that the OM dissolved by the oxalate extraction has the same C:N ratio as that in bulk fraction. This assumption cannot be fully justified but would be a reasonable approximation for the purpose of assessing the trends because a plot of the C:N ratio of PP-extractable phase against that of
175    bulk soil C:N (regression through the origin) showed significant positive correlation ($r^2$=0.89, p<0.0001) with the slope close to one (1.25 with 95% confidence interval of 1.15-1.32). Total organic C and N concentrations in the isolated fractions and bulk samples were analyzed by an elemental analyzer (Flash2000 Thermo Fisher Scientific Inc., USA).

## 2.5 Statistics

Linear regression analyses between extractable metals and DOC were done using JMP software (version 8.0.1, SAS
180    Institute, Cary, NC. USA). Density-dependent change in the proportion of total C in each fraction explained by the association with PP- and OX-extractable phases ($[DOC_{PP}+DOC_{OX}]$:TC) was modeled for each soil group using polynomial functions using JMP software.

## 2.6 Peak density determination

For each soil sample, we determined the particle density at which the metal concentration from each extraction was
185    highest (termed as "peak density") using two approaches. First, we simply selected the density fraction where the metal concentration was the highest among the fractions for a given soil and used its midpoint (e.g., 2.1 g cm$^{-3}$ for 2.0-2.2 g cm$^{-3}$ fraction) as the peak density. The actual peak density is not necessarily its mean especially for the samples separated into a

smaller number of fractions. Thus, as a second approach, we also estimated the peak density by fitting a normal distribution curve to the metal concentrations per fraction against particle density for each soil (Fig. A1, left panels). The majority of soil

190 samples fitted well, though we had to remove the data points from the lowest- and highest-density fractions in some cases (Fig. A1). For instance, OX and DC-extractable metal concentrations in the highest density fractions were quite high for non-allophanic Andisol samples due presumably to magnetite. Thus those data points were not used for the fitting. Similarly, we eliminated the lowest one or two density fractions of PP- and OX-extractable metal concentration data from six samples from the crystalline mineralogy group. Eliminating these data points (Fig. A1) was done only to enable fitting a normal distribution

195 (on average $r^2 = 0.90$-$0.98$, Fig. A2a). The mean of the normal distribution for each extraction/soil was used as the second estimate of peak density. We also determined the mass-weighted particle density at which the metal was most concentrated. After calculating the metal distribution along the density gradient (i.e., [metal concentration] x [mass fraction]), the two approaches above were applied to determine the peak density for each soil sample and each extractable metal phase. A normal distribution fitted well for most samples (Fig. A1 right panels, Fig. A2b).

## 2.7 Scanning electron microscopy

Isolated density fractions from selected soil samples were observed by SEM (SU1510, Hitachi high-technologies, Tokyo, Japan). Subset of freeze-dried density fractions were re-dispersed in ultrapure water by weak sonication ($<10$ J mL$^{-1}$), deposited on carbon tape, and were Pt-Pd coated prior to the observation.

## 3 Results

## 3.1 Recovery after sequential density fractionation

Our density fractionation procedure showed largely reasonable recovery of mass, C, and N for the 23 soil samples studied (Table 2). While the recovery of the metals assessed by PP-, OX-, and DC sequential extractions were generally good, the variation among the soils was larger (Table 2) as some soil samples and metal phases showed poor recoveries. Possible sources of errors are (i) the small sample mass used for the extractions, (ii) additive errors from the sequential extractions, and (iii) the

210 small sizes of targeted pools. For example, the recovery worsened for DC-extractable Al and Si pools following PP and OX extractions. Incomplete removal of colloidal Fe and Al phases likely explains higher metal recovery from Andisol samples ($118 \pm 36\%$) compared to non-Andisol samples ($84 \pm 12\%$) in PP extraction. The factors affecting the poor recovery with the sequential extraction approach were discussed in more detail elsewhere (Wagai et al., 2018). We considered that the obtained recoveries are tolerable for assessing the general patterns of the metals and OM across the density fractions.

## 3.2 Concentration of C, N, and extractable metals along particle density gradient

The C concentration was highest in the lowest-density fraction, declined with increasing density up to ca. 2.5 g cm$^{-3}$, and remained low at higher densities for all the studied soils (Fig. A3a). Similarly, C:N ratio showed a progressive decline with

increasing density (Fig. A3b). While the majority of the samples showed very low C and C:N ratio in the fractions higher than ca 2.5 g cm$^{-3}$, a few samples showed a slight increase towards the highest density fraction.

220   The pedogenic metal concentration (Al+0.5Fe) generally showed a unimodal pattern along the particle density gradient with some distinct patterns among the four soil groups (Fig. 1, also see Fig. A1 left panels for individual soils). Allophanic Andisol group showed higher OX- and DC-extractable metals (metal$_{OX}$, metal$_{DC}$) especially in an intermediate density range, whereas non-allophanic Andisol and Spodosol groups were characterized by high concentrations of PP-extractable metals (metal$_{PP}$). As expected, the crystalline mineralogy group showed the lowest levels of metal$_{PP}$ and metal$_{OX}$ with moderate

225   amounts of metal$_{DC}$ from highly-weathered soil samples. Two exceptions to the general unimodal pattern were present. For metal$_{PP}$, three soil samples showed their peak metal concentrations at the lowest density. For metal$_{OX}$, three samples of non-allophanic Andisols showed the highest metal (esp. Fe) concentrations at the highest density due presumably to the presence of Fe-bearing primary minerals such as magnetite. Even in the soils relatively low in specific metal phases (e.g., the crystalline mineralogy group low in metal$_{PP}$ and metal$_{OX}$, and the non-allophanic Andisol and Spodosol groups low in metal$_{OX}$ and

230   metal$_{DC}$), the highest metal concentrations were found at an intermediate density range (Fig. A1 right panels).

Similar patterns were shown when assessing the distribution of the metals along the density gradient by accounting for mass distribution (Fig. A1 right panels). The unimodal pattern remains for most samples, indicating that the major portions of respective metal phases accumulated in an intermediate-density range. However, the dominant metal phase clearly differed among the soil groups. In the allophanic Andisol group, $63 \pm 9\%$ of the total extractable metal was present in OX-extractable

235   phase. On the other hand, the non-allophanic Andisol and Spodosol groups showed that $59 \pm 25\%$ and $75 \pm 14\%$ of the total extractable metals, respectively, were accounted for by PP-extractable phase. In the crystalline mineralogy group, DC-extractable phase tended to be higher ($41 \pm 14\%$ of the total extractable metal).

The Al:Fe molar ratio was highest in metal$_{PP}$ phase ($4.7 \pm 4.3$, mean $\pm$ SD) followed by metal$_{OX}$ phase ($2.6 \pm 1.9$) and, expectedly, lowest in metal$_{DC}$ phase ($0.4 \pm 0.3$) across all soils and their fractions. Several patterns were identified (Fig. A4).

240   First, relative enrichment of Fe in metal$_{OX}$ and metal$_{DC}$ phases was evident in the highest density fractions due presumably to the dissolution of crystalline Fe oxides. Second, from the low to intermediate density up to 2.3 g cm$^{-3}$, the Al:Fe ratio remained relatively constant with some exceptions. The allophanic Andisol group showed relative Al enrichment at around 1.8 g cm$^{-3}$ for PP-extractable phase and at around 2.0-2.3 g cm$^{-3}$ for metal$_{OX}$ phase. The non-allophanic Andisol group showed the Al enrichment towards low density for all extractable phases. For the other soil groups, similar Al enrichment was found in some

245   samples while others showed constant Al:Fe ratios. Nevertheless, the density at which the metal concentration reached its peak (peak density) was quite similar between Fe and Al (data not shown). We thus examined the extractable Fe and Al together (i.e., Al+0.5Fe) for most of the subsequent analyses.

Peak densities for pedogenic metal concentrations were found at an intermediate density range for all soil samples studied with some variations among the extractable phases. The peak densities of metal$_{PP}$ phase were more variable compared to

250   metal$_{OX}$ and metal$_{DC}$ phases (Fig. 2). In particular, two C-rich samples (C-3, C-7) had the fitted peak density of metal$_{PP}$ at <1.5 g cm$^{-3}$ (Fig. A1). The medians (and lower to upper quartiles) of the measured peak density among the 23 soil samples for PP-,

OX- and DC-extractable metal phases were 1.7 (1.7-2.0), 2.1 (2.1-2.3), and 2.2 (2.1-2.3) g cm$^{-3}$, respectively (Fig. 2). Similarly, their means were 1.8, 2.2, and 2.2 g cm$^{-3}$. The peak densities estimated by the normal distribution fitting also showed comparable values. Thus, the peak densities of all three extractable phases were <2.3 g cm$^{-3}$. The metal$_{PP}$ phase showed its

255   peak consistently lower by 0.3-0.4 g cm$^{-3}$ than metal$_{OX}$ and metal$_{DC}$ phases (Fig. 1 and 2).

The concentrations of C co-dissolved during the initial PP and OX extractions (DOC$_{PP}$ and DOC$_{OX}$) correlated positively with the extractable metal concentrations (Fig. 3a-f). Coefficients of determination were highest for Al$_{PP}$+0.5Fe$_{PP}$ (r$^2$=0.75, p <0.0001) followed by Al$_{PP}$ (0.66, <0.0001) and then Fe$_{PP}$ (0.56, <0.0001). Importantly, the positive DOC$_{PP}$-Al$_{PP}$ and/or DOC$_{PP}$-Fe$_{PP}$ relationship persisted across the density fractions within each soil although the correlation was not significant for 5 out

260   of 23 samples (Fig. A5). The DOC$_{PP}$:Al$_{PP}$ mass ratio (i.e., slope of the regression lines) ranged from 2.9 to 28.2 (mean: 7.9, SE: 1.6).

Similarly, the organic matter co-dissolved by the oxalate extraction (DOC$_{OX}$) was positively related to metal$_{OX}$ owing largely to the allophanic Andisol samples (Fig. 3d-f). Simple linear regression of DOC$_{OX}$ against Al$_{OX}$, Fe$_{OX}$, and Al$_{OX}$+0.5Fe$_{OX}$ concentrations among all samples showed the strongest control by Al$_{OX}$ (r$^2$=0.66) followed by Al$_{OX}$+0.5Fe$_{OX}$ (r$^2$=0.60) and

265   then Fe$_{OX}$ (r$^2$=0.39, p <0.0001). When assessed for individual soils, the positive C-metal relationship (mostly only with Al$_{OX}$) persisted for 8 out of the 14 Andisol samples but no positive relationship was present for the rest of soils (Fig. A6). The range for DOC$_{OX}$:Al$_{OX}$ mass ratio was 0.13-0.34 and that of DOC$_{OX}$:(Al$_{OX}$+0.5Fe$_{OX}$) was 0.11-0.22 for these Andisol samples (data not shown). These ratios were roughly 10-50 times less than that from PP-extractable phase.

The proportion of total C in each density fraction co-dissolved by initial PP and by the sum of PP and subsequent OX

270   extractions showed an increasing trend with increasing particle density (Fig. 4). Despite high variability especially towards higher density fractions, the increasing trend with density was fitted by a polynomial curve for each of the four soil groups separately (Table A1). The three soil groups having high extractable metals tended to have higher proportions of extractable C compared to the crystalline mineralogy group. The allophanic Andisol group, which was characterized by higher Al$_{OX}$ and Fe$_{OX}$ concentrations, showed that appreciable amounts of OM were co-dissolved by the dissolution of metal$_{OX}$ phase (Fig. 4a).

275   In contrast, the non-allophanic Andisols and Spodosol groups showed that nearly all the extractable C was released by the initial PP extraction. The non-allophanic Andisol group having characteristically high Al$_{PP}$ and Fe$_{PP}$ concentrations showed that a quarter up to nearly all of the C present in the higher-density fractions was co-dissolved by the initial PP extraction (Fig. 4b).

### 3.3 Distribution of mass, organic matter and extractable metal phases along the density gradient

280   The density fraction which accounted for the largest portion of bulk soil mass was in 2.2-2.6 g cm$^{-3}$ density range and its median (and lower-upper quartiles) was 2.5 (2.2-2.6) g cm$^{-3}$ among the 23 soil samples (Fig. 5). Carbon distribution, calculated by multiplying the C concentration by the fractional mass for each density fraction, showed its peak in significantly lower yet still intermediate density range (Fig. 5) with the median of 2.1 (1.9-2.2) g cm$^{-3}$. The data points at 1.4 g cm$^{-3}$ were from three samples (A-1, S-1, and C-7) having very high total C due to high OM input or reduced decomposition under cooler climate.

SOIL
Discussions

285    The extractable metals were also mainly concentrated in the intermediate-density range (Fig. A1 left, Fig. 5b), which is statistically indistinguishable from C peak as a whole sample set (n=23). The medians (and lower-upper quartiles) of the peak density for PP-, OX-, and DC-extractable phases were 2.1 (2.1-2.2), 2.1 (2.1-2.3), and 2.2 (2.1-2.4) g cm$^{-3}$, respectively. In contrast with the concentration-based patterns (Fig. 2), no clear difference was found between PP- and the other two extractions due to the small mass contribution of the lower-density fractions where PP-extractable metal concentration was higher (Fig.

290    A1a).

### 3.4  SEM observation of meso-density fractions

Clear shift in dominant particle type from plant detritus (POM) in the lowest-density fraction to coarse mineral grain in the highest-density fraction was observed for the two soils from the crystalline mineralogy group we selected. We assessed three intermediate-density fractions where majority of metals and OM reside in detail. In both soils, 2.0-2.2 g cm$^{-3}$ fraction

295    was abundant in fragmented POM as well as aggregates (Fig. 6a, d) while the material in 2.2-2.4 g cm$^{-3}$ fraction appeared largely aggregated (Fig. 6b, e). At closer look on the surface of these aggregates and POM, clay platelets (<5 μm) were visible. The higher-density fractions had more mineral grains with clean surfaces although some grains in 2.4-2.6 g cm$^{-3}$ fraction were aggregated or showed rough surfaces (Fig. 6c, f). The size of these aggregates in these fractions ranged from a few tens to hundreds μm in diameters. Similar features were found for the density fractions in one of the studied Andisols (A-3, Wagai et

300    al., 2014).

### 4  Discussion

### 4.1  Fe and Al phases extracted by the three reagents

The metals released by PP, OX, and DC extractions only *roughly* correspond to specific metal phases present in the soil as these extractions are not highly selective (Parfitt, 2009; Rennert, 2019). This approach, nevertheless, remains important as

305    the extractable metal contents often show significant correlation with soil C storage and turnover times (Masiello et al., 2004; Percival et al., 2000; Porras et al., 2017; Torn et al., 1997; Wada and Higashi, 1976). It is thus critical to elucidate the nature of these metal phases including their localization, which aids resolving the gap between commonly-used mathematical models and the current understanding of soil C dynamics (Blankinship et al., 2018). Compared to common single extraction, sequential extraction approach may allow better assignment of different Fe and Al phases (Dai et al., 2011; Shang and Tiessen, 1998). It

310    is generally assumed that the PP extraction mainly dissolves organo-metal complexes (Bascomb, 1968; Takahashi and Dahlgren, 2016), whereas the OX and DC extractions target dissolution of short-range-order minerals and crystalline iron oxides, respectively (e.g., Inagaki et al., 2020; Lawrence et al., 2015; Shang and Tiessen, 1998). Pyrophosphate extraction data requires particularly  cautious interpretation due to the OM dissolution by high alkalinity (pH 10) and the dispersion or dissolution of colloidal and low-crystallinity Fe and Al oxide phases (Coward et al., 2018; Kaiser and Zech, 1996; Lawrence

315 et al., 2015; Schuppli et al., 1983; Shang and Tiessen, 1998; Wagai et al., 2013). However, the significant $DOC_{PP}$-$metal_{PP}$ (esp. $DOC_{PP}$-$Al_{PP}$) correlations found across the soils (Fig. 3a-c) and, to a limited extent, among the fractions within soils (Fig. A5) imply the predominance of strong OM-metal association phases such as organo-metal complexes in PP extracts because the potential artifacts, if occurring significantly, would have prevented the emergence of the proportional relationship. Most of the studied soils showed significant C-metal correlation with high $DOC_{PP}$:$Al_{PP}$ molar ratios (mean ± SE: 17.8 ± 3.5, range: 6.6-

320 63.3) and $DOC_{PP}$:$Fe_{PP}$ ratios (75.6 ± 18.0, range: 17.6-168, Fig. A5) in agreement with previous studies (Heckman et al., 2018; Wagai et al., 2013). While C:metal ratios of synthesized organo-metal associations vary widely depending on experimental conditions, higher ratios indicate dominance of organo-metal complexes over adsorptive association with metal oxides (Wagai and Mayer, 2007). In laboratory coprecipitation experiments, a C:Fe molar ratio exceeding one led to organic encapsulation of Fe oxide particles (Kleber et al., 2015). Takahashi and Dahlgren (2016) estimated the C:metal molar ratio of 8.3 for organo-

325 metal complexes in Andisols. We thus regard the PP-extractable phase as a mixture consisting largely of organo-metal complexes and their coprecipitates with varying amounts of alkali-soluble and desorbable OM and non-centrifugeable colloidal Fe/Al oxide phases.

The OX-extractable metal phase is more likely influenced by short-range-order minerals (Parfitt and Childs, 1988; Rennert, 2019). We found strong positive correlation between $Al_{OX}$ and $Si_{OX}$ ($r^2$=0.76-0.99) with relatively constant $Al_{OX}$:$Si_{OX}$ molar

330 ratio for each soil group: 4.4 (allophanic Andisols), 4.8 (non-allophanic Andisols), 7.7 (Spodosols), and 8.4 (crystalline mineralogy group). Short-range-order aluminosilicates commonly found in Andisols and Spodosols have a molar ratio of 1-2, but possibly up to 4 for Al-rich allophane (Dahlgren et al., 1993). The OX-extractable phase in the studied soil fractions may also contain poorly-crystalline gibbsite which can form rapidly in OM-rich, acidic soil environment (e.g., Heckman et al., 2013). The source of $Al_{OX}$ and $Si_{OX}$ in the crystalline mineralogy group is less clear but likely to include interlayer components

335 of 2:1 clay such as hydroxy Al polymers and aluminosilicates (Barnhisel and Bertsch, 1989; Wada and Kakuto, 1983) as well as amorphous gibbsite and silica (Drees et al., 1989). Most $Fe_{OX}$ phase is attributable to ferrihydrite and colloidal goethite for lower-density fractions, and less-crystalline Fe oxides as well as magnetite - a primary mineral that associates little with OM - for higher density fractions (Cornell and Schwertmann, 2003; Parfitt and Childs, 1988; Rennert, 2019). The DC-extractable metal phase obtained after PP and OX extractions largely represents crystalline iron oxides and coprecipitated Al phases

340 (Cornell and Schwertmann, 2003).

The Al:Fe molar ratio of the extracts was relatively constant along the particle density gradient in some of the soils (Fig. A4), implying coprecipitation of organo-Fe and organo-Al phases. The other soils, mostly in Andisol and Spodosol groups, showed density-dependent patterns. Some of the allophanic Andisol samples, all of the non-allophanic Andisol samples and one of the two Spodosol samples showed higher Al:Fe ratios towards lower-density fractions especially in $metal_{PP}$ and $metal_{OX}$

345 phases (Fig. A4a-c). These higher Al:Fe ratios may be explained by higher capability of Al ions to form insoluble complex with organic ligands under low pH and low metal:C ratio conditions (Nierop et al., 2002). In addition, the lower density of organo-Al coprecipitates (1.7 g cm$^{-3}$) than that of organo-Fe ones (2.5 g cm$^{-3}$, Kaiser and Guggenberger, 2007) may account for the observed higher Al:Fe ratios.

11

## 4.2 Pedogenic metal enrichment at intermediate (meso) density range

350   The concentrations of extractable metal phases peaked at intermediate densities along the soil particle density gradient (Fig. 2, Fig. A1 left panels). Their dominance below the density cutoff of 2.4 g cm$^{-3}$ can be explained only by their association with OM which has a much lower density (~1.4 g cm$^{-3}$), supporting our hypothesis. While the cutoff densities for the intermediate range are somewhat arbitrary, we define the range between 1.8 and 2.4 g cm$^{-3}$ as meso density for following reasons: (i) a strong decline in OM concentration and C:N ratio above ~1.8 g cm$^{-3}$ (Fig. A3a,b) suggests a major shift in OM

355   source from plant detritus to microbially-altered compounds as shown previously (e.g., Baisden et al., 2002), (ii) both the concentrations and distributions of the extractable metals began to increase at >1.8 g cm$^{-3}$ (Fig. A1), and (iii) most soil minerals have density >2.4 g cm$^{-3}$ (see Introduction). Thus, the meso-density fractions are characterized by enrichment of pedogenic Fe and Al phases and their association with microbially-altered OM. The extractable metal phases in the meso densities made up less than one-fifth of soil masses and the rest consisted largely of other minerals (e.g., crystalline clays) to form

360   microaggregates resistant to mechanical shaking (Fig. 6). The meso-density enrichment of the metals thus implies their preferential association with OM relative to the other minerals.

Within the meso-density range, we found clear localization of different metal phases. The peak density of metal$_{PP}$ concentration had the median of 1.8 (1.7-2.0) g cm$^{-3}$ which was lower by 0.3-0.4 g cm$^{-3}$ (on average) relative to metal$_{OX}$ and metal$_{DC}$ across the soils (Fig. 2, Fig. A1 left). This difference remained the same when assessing Fe and Al separately. The

365   lower peak density of metal$_{PP}$ can result either from the inherent low density of this phase as indicated by the high C:metal ratios (see Section 4.1, Fig. 3a-c) or from its attachment to low-density particles. The latter implies that metal$_{PP}$ phase was preferentially associated with lower-density aggregates such as clay-covered POM (Fig. 6a, c), which would account for the presence of Fe$_{PP}$ phase despite its higher density than Al$_{PP}$ phase.

Progressive changes in the concentrations of both organic and inorganic (mineral) phases along the density gradient (Fig.

370   1, Fig. A3a) are depicted for an idealized soil (Fig. 7a). While distinguishing between plant-derived POM in low-density fraction and mineral-associated OM (MAOM) in high-density fraction within bulk soil is a critical first step (Lavallee et al., 2020; Sollins et al., 1999), the transition from POM to MAOM is rather continuous and the latter contains a wide array of OM-mineral associations (Hatton et al., 2012; Jones and Singh, 2014; Sollins et al., 2009; Turchenek and Oades, 1979; Wagai et al., 2018) as conceptualized in "Soil Continuum Model" of soil OM formation (Lehmann and Kleber, 2015). The higher-

375   density fractions (e.g., >2.4 g cm$^{-3}$) are increasingly dominated with primary minerals and Fe-bearing minerals including crystalline Fe oxides (Jones and Singh, 2014; Sollins et al., 2009) with small amounts of N-rich OM (Fig. A3). The lower-density fractions, on the other hand, hold increasing amounts of POM with appreciable levels of PP-extractable organo-metal phases especially at around 1.8 g cm$^{-3}$ range (Fig. 1, 2). In the meso-density fractions (1.8-2.4 g cm$^{-3}$), where the major portions of OM and extractable metals were located, significant portions (20% up to nearly 100%) of the OM therein were co-dissolved

380   by PP and OX extractions (Fig. 4). By applying similar sequential extraction method to four soil profiles of contrasting mineralogy, Heckman et al. (2018) reported, on average, 70% of total C was extractable. These extractable OM possibly

SOIL Open Access
Discussions
EGU

existed in metal-bound forms (Coward et al., 2017; Wagai et al., 2013; Zhao et al., 2016). The remaining, non-extractable OM in the meso-density fraction is presumably stabilized by mechanisms other than simple adsorptive association with the extractable metal phases.

385 **4.3 Organo-metal association, aggregation, and OM stabilization**

Organo-metal associations take place at multiple spatial scales within a bulk soil. Organo-metallic complexation, sorption and co-precipitation occur at molecular to colloidal scales (Kleber et al., 2015). Current density fractionation results, on the other hand, suggest that the extractable metals and associated OM contribute to the formation of meso-density aggregates having a few tens to hundreds of μm in diameter (Fig. 6). At the aggregate scale, organo-mineral interactions occur with much

390 higher level of complexity (Keil and Mayer, 2014; Totsche et al., 2017). Here, we discuss how colloidal-scale interaction of metals and OM may be linked with micron-scale aggregate formation to account for the observed density-dependent patterns.

The observed proportionality between extractable metal phases and associated OM among the density fractions gives some hints to bridge between the colloidal and larger-scale associations. Significant C-metal correlations in PP- and OX-extractable phases, previously found across a range of bulk soils (Wagai et al., 2013), were shown among the density fractions

395 (Fig. 3) and even within each soil in many cases (Fig. A5, A6). Specifically, positive $DOC_{PP}$-$metal_{PP}$ correlation (largely $DOC_{PP}$-$Al_{PP}$) was found for all soils except for three samples from the crystalline mineralogy group (Fig. A5) while such correlation for the subsequent OX extraction was limited to 8 out of the 14 Andisol samples (Fig. A6). Relatively constant C:metal ratios across the density fractions imply that the organo-metal association formed in the field remained intact as a physical unit during the fractionation steps and these units were distributed among the fractions. These organo-metal units

400 themselves are presumably present as colloid-sized "nanocomposites" (Fig. 7b) consisting of precipitated organo-metal complexes (i.e., $metal_{PP}$ phase) and, at least in the case of Andisols, OM-sorbed metal oxides (i.e., $metal_{OX}$ phase), such as those identified in soils using high resolution imaging techniques (Asano et al., 2018; Wen et al., 2014). Another feature is that these nanocomposites must be attached to larger particles containing some combination of low-density OM, high-density mineral, or more of each other. Without sufficient size, Stokes Law predicts that they would have remained in density liquid

405 and lost during the centrifugation step.

We hypothesize that these organo-metal-rich nanocomposites function as a glue or effective binding agent (Asano et al., 2018) and promote ternary associations of OM, metal, and clays (Wagai and Mayer, 2007), as depicted in Figure 7b. In fact, the meso-density materials were largely present as microaggregates with abundant clays on their surfaces (Fig. 6). For the two soil samples (A-3, C-4) that we further size-fractionated following the density fractionation, 59-84% of the mass in the meso-

410 density fractions consisted of <2 μm sized particles (isolated after maximum dispersion by sonication) that were enriched in the extractable metals relative to bulk samples (unpublished data) in support of our hypothesis. How do these nanocomposites form and function? The Al and Fe are trivalent metals and can act as (monomeric or polynuclear) glue between different organic ligands, particles, and surfaces. An organic particle or coating may stick to a mineral surface via van der Waals interactions, but become aggregated to other organic particles via a polyvalent metal connection. Furthermore, monomeric Fe

415    and Al can form various ternary complexes in the presence of OM and other dissolved inorganic species found in soil solution such as Ca and Si, thereby preventing their polymerization (Adhikari et al., 2019; Tamrat et al., 2019; Yang et al., 2017). These organo-metal-rich, mixed-phase nanocomposites, acting as glues (organo-metallic glue hypothesis), can give a mechanistic explanation for the moderately strong C-metal correlations among the density fractions (Fig. 3, Fig. A5, A6) as well as for the dominance of OM, metal, and presumably clay in the meso-density range (Fig. 5, A1).

420    Such micro-scale aggregation can enhance OM stability by reducing the accessibility of microbes, exo-enzymes, and/or e- acceptors (Balesdent et al., 2000; Keil and Mayer, 2014; Lehmann et al., 2007; Sollins et al., 1996). Among the pedogenic metal phases, crystalline Fe oxides (roughly corresponds to metal$_{DC}$ phase) strongly enhance microaggregation particularly in highly weathered soils (e.g., Shang and Tiessen, 1998). This metal phase can protect relatively small amounts of OM for a prolonged time (e.g., Eusterhues et al., 2003; Mikutta et al., 2006). Short-range-order mineral could also contribute to

425    aggregation and thus physical protection of OM within such mineral matrix. Microaggregates in Andisols (esp. metal$_{OX}$-rich ones) show high physical stability (Shoji et al., 1993) even against wet oxidation and reductive dissolution treatments (Churchman and Tate, 1986). Stable ternary associations of OM, low-crystallinity Fe oxide, and microporous allophane in an Andisol has been hypothesized (Filimonova et al., 2016). A portion of soil extractable Fe such as low-crystallinity Fe oxyhydroxide, and presumably associated OM, can survive harsh dithionite extraction (Coward et al., 2018), in some cases,

430    due to protective effect of metal$_{OX}$ phases. Even after strong dispersion by sonication (up to 1500 J ml$^{-1}$), 60-70% of total C and extractable metals in Andisols remained in the meso-density fractions (Basile-Doelsch et al., 2007; Wagai et al., 2015) that were largely present as micron- and submicron-sized aggregates (Asano and Wagai, 2014; Asano et al., 2018). Similarly, the main C storage location in tropical Ferrasols was sonication-resistant particles that were characterized by slightly higher density (2.45-2.8 g cm$^{-3}$), enrichment of halloysite, and resistance to ~200 yrs of cultivation (Basile-Doelsch et al., 2009).

435    Compared to these metal oxide phases, organo-metal complexes are more labile, for instance, with change in pH (Takahashi and Dahlgren, 2016). Thus their contribution to aggregation may be lower although this phase can be physically occluded within stable microaggregates. Faster turnover (more $^{14}$C enrichment) of PP-extractable C compared to the C associated with other mineral phases (Heckman et al., 2018) as well as the metal$_{PP}$ enrichment at lower density (Fig. 1, 2) support this view. While relative importance of specific metal phases remains to be elucidated, these extractable metals likely contribute to OM

440    stabilization by promoting aggregation via organo-metallic glues as well as by direct organo-metal interaction via complexation and adsorption.

### 4.5 Co-localization of metal and microbially-altered OM at meso-density fraction

We further considered the distributions of metal and OM along the density gradient to translate the observed results into field-level processes. Their distributions are determined by two variables: mass distribution and the concentration of the

445    respective elements. The peak density of mass distribution was quite variable among the studied soils (Fig. 5), which will be further examined in our companion study (Kajiura et al., in prep.). Consequently, the peak densities of metal phases were also moderately variable. The mean peak densities of both C and all metal phases were, however, ~2.1 g cm$^{-3}$ (Fig. 5). In fact, the

meso-density range (1.8-2.4 g cm$^{-3}$) accounted for 59 ± 14% and 64 ± 15% (mean ± SD) of total C and N, respectively, among the studied soils. Similarly, more than half of the total extractable metals were in the meso-density range (65 ± 17% of Fe$_{PP}$,

450    63 ± 15% of Al$_{PP}$, 56 ± 14% of Fe$_{OX}$, 70 ± 13% of Al$_{OX}$, 61 ± 17% of Fe$_{DC}$, and 66 ± 15% of Al$_{DC}$). The meso-density co-localization of OM and the extractable metals found here thus suggest that metal binding via multiple physico-chemical processes discussed above contributes to the stability of pedogenic metal phases against leaching/dissolution and that of OM against biological degradation. Our view is consistent with C and N isotope tracer studies that identified meso-density fractions as the main reservoir of stabilized C across a wide range of soils (Baisden et al., 2002; Crow et al., 2014; Hatton et al., 2012;

455    Sollins et al., 2009; Wagai et al., 2018; Jones and Singh, 2014) with an exeption of Fe-rich weathered soils where >2.4 g cm$^{-3}$ fractions store more C due to the abundance of heavy minerals (Jones and Singh, 2014; Sollins et al., 2009).

The co-localization of OM and metals is illustrated for the three forest soils developed through contrasting pedogenesis (Fig. 8). In the tropical Ultisol, DC-extractable phase accounted for greater proportions of total extractable metal than the other two soils (Fig. 8a). Accordingly, this phase explained the majority of the OM extractable by PP, OX, and DC (Wagai et al.,

460    2013). The spodic horizon sample under cooler climate stored more C in lower density fractions and held major portions of metals as PP-extractable phase (Fig. 8b) in agreement with podzolization concept (Lundström et al., 2000). The allophanic Andisol held much higher amounts of extractable metals and C than the other two soils (Fig. 8c). Co-localization at a narrower density range in the Andisol can be attributable to higher contents of organo-metallic glue.

### 4.5 Implications

465    The similar distributions of OM and extractable Fe and Al found here (Fig. 5, 8, A1) imply a common set of processes that promote the formation of organo-metal associations across a range of pedogenic environments. Almost all samples showed a unimodal distribution with the peaks in the meso-density range (Fig. 1, 2, and Fig. A1). The three processes operating at a fundamental level are (1) the production of microbially-altered OM from the original low-density plant detritus, (2) the release of metals from high-density, weatherable minerals, and (3) the formation of organo-metal-rich nanocomposites and concurrent

470    incorporation of low- and high-density materials (most importantly, clays) into meso density via their gluing properties – the organo-metallic glue hypothesis (Fig. 8) .

From the organic side, the most consistent change along the particle density gradient was the progressive decline in C:N ratio and OM concentration from low to high-density fractions (Fig. A3), which is generally explained by the shift from POM to microbially-processed compounds (Baisden et al., 2002; Gunina and Kuzyakov, 2014). Microbially-driven, oxidative

475    depolymerization increases the solubility, the number of ionized functional groups (esp. carboxylic groups), and acidity thereby enhancing the reactivity of remaining OM with metals and mineral surfaces (Heckman et al., 2013; Kleber et al., 2015). The accumulation of the pedogenic metal phases from low to meso density fractions (Fig. 2, Fig. A1) thus suggests that oxidative depolymerization of POM appears to be necessary for the organo-metal associations. From the mineral side, metals released by weathering can readily bind to organic ligands. For instance, negatively-charged bacterial cell surface attracts metal cations,

480    which leads to the nucleation and precipitation of low-crystallinity Fe oxyhydroxides and aluminosilicates (Ferris et al., 1989;

Urrutia and Beveridge, 1994). Tamrat et al. (2019) showed nano-sized Fe-Al-Si coprecipitate formation from biotite weathering solution in the presence of low-molecular organic acid. These reactions likely promote the formation of the nanocomposites having a relatively narrow range of OM:metal ratios that can act as relatively persistent glue to bind soil particles, most importantly phyllosilicate clays that themselves strongly bind with OM.

485     The three processes identified (Fig. 9) are ultimately driven by the factors driving pedogenesis – physicochemical forces (heat, water, acidity) and biological activity. Then the environmental conditions promoting the three processes in balance would lead to local maxima of the organo-metallic glue and meso-density aggregates (see Fig. A7 and the discussion therein). Such condition at the global scale includes acidic soils under wetter climate (Rasmussen et al., 2018) especially with the parent materials that are abundant in weatherable minerals. At the pedon scale, the interface of O/A horizons or the B horizons that

490     experience podzolization would fit with this condition. At smaller scales, micro spots having redox fluctuation and rhizosphere likely promote the organo-metallic glue formation due to the abundance of organic ligands and active dissolution/precipitation of Fe and other mineral phases (Chen et al., 2020; Garcia Arredondo et al., 2019; Keiluweit et al., 2015; Yu, 2018). The current view and the growing evidence on rapid formation of various organo-metal-mineral associations at submicron scale (e.g., Basile-Doelsch et al., 2015; Garcia Arredondo et al., 2019; Heckman et al., 2013) suggest that the concept of soil C saturation

495     and soil's capacity to protect C based on clay and silt contents (e.g., Six et al., 2002) require refinement.

        Our results and proposed hypothesis may help to integrate some of the important findings and concepts in the literature. Predominance of stabilized OM in organo-mineral fractions (e.g., <20 μm size class or meso-density range) has been shown by physical fractionation studies (e.g., Christensen, 2001; Six et al., 2000; von Lützow et al., 2007) but the involvement of pedogenic metal phases was much less studied. Protective effects of phyllosilicate clays (e.g., Barré et al., 2014) and pedogenic

500     metal phases (e.g., Porras et al., 2017; Wagai and Mayer, 2007) on OM are likely to occur concurrently, and possibly synergistically, within meso-density microaggregates. Enrichment of certain clay minerals in meso-density fractions (e.g., smectite in a Vertisol, kaolinite in Spodosol and Oxisol, Jones and Singh, 2014) and enhanced physical stability of clay aggregates by the incorporation of goethite particles (Dultz et al., 2019) support this idea. Aggregate hierarchy concept recognized the role of low-crystallinity mineral phases and microbial compounds as persistent binding agents (Tisdall and

505     Oades, 1982) but not their interaction or formation pathways. With new analytical techniques and methodologies, our undernding of microaggregate formation (e.g., Lehmann et al., 2007; Totsche et al., 2017) and molecular-scale interaction of OM, metal, and mineral (e.g., Kleber et al., 2007; Tamrat et al., 2019) is advancing. We believe that a remaining key question is how these molecular scale interactions are related to soil physical fractions and the formation of hierarchical aggregate structure. The current finding provided some insights to this end. Further efforts to fill the scale gap will be important to better

510     understand soil's protective capacity to store OM and for the development of more mechanistic biogeochemical models.

SOIL Discussions

Open Access

EGU

## Acknowledgments

## References

Adhikari, D., Sowers, T., Stuckey, J. W., Wang, X., Sparks, D. L., and Yang, Y.: Formation and redox reactivity of ferrihydrite-organic carbon-calcium co-precipitates, Geochimica et Cosmochimica Acta, 244, 86-98, https://doi.org/10.1016/j.gca.2018.09.026, 2019.

Anthony, J. W., Bideaux, R. A., Bladh, K. W., and Nichols, M. C.: Volume III. Halides, Hydroxides, Oxides., Handbook of Mineralogy, Mineralogical Society of America, Chantilly, VA 20151-1110, USA., 1997.

Asano, M., and Wagai, R.: Evidence of aggregate hierarchy at micro- to submicron scales in an allophanic Andisol, Geoderma, 216, 62-74, http://dx.doi.org/10.1016/j.geoderma.2013.10.005, 2014.

Asano, M., Wagai, R., Yamaguchi, N., Takeichi, Y., Maeda, M., Suga, H., and Takahashi, Y.: In Search of a Binding Agent: Nano-Scale Evidence of Preferential Carbon Associations with Poorly-Crystalline Mineral Phases in Physically-Stable, Clay-Sized Aggregates, Soil Systems, 2, 32, 2018.

Baisden, W. T., Amundson, R., Cook, A. C., and Brenner, D. L.: Turnover and storage of C and N in five density fractions from California annual grassland surface soils, Glob. Biogeochem. Cycle, 16, 1117, 10.1029/2001GB001822, 2002.

Balesdent, J., Chenu, C., and Balabane, M.: Relationship of soil organic matter dynamics to physical protection and tillage, Soil and Tillage Research, 53, 215-230, https://doi.org/10.1016/S0167-1987(99)00107-5, 2000.

Barnhisel, R., and Bertsch, P.: Chlorites and hydroxy-interlayered vermiculite and smectite, in: Minerals in Soil Environments, 2nd ed., edited by: Dixon, J. B., Weed, S.B., Soil Science Society of America Book Series, Soil Science Society of America, 729-788, 1989.

Barré, P., Fernandez-Ugalde, O., Virto, I., Velde, B., and Chenu, C.: Impact of phyllosilicate mineralogy on organic carbon stabilization in soils: incomplete knowledge and exciting prospects, Geoderma, 235–236, 382-395, http://dx.doi.org/10.1016/j.geoderma.2014.07.029, 2014.

Bascomb, C. L.: Distribution of pyrophosphate-extractable iron and organic carbon in soils of various groups, Journal of Soil Science, 19, 251-268, 10.1111/j.1365-2389.1968.tb01538.x, 1968.

545 Basile-Doelsch, I., Amundson, R., Stone, W. E. E., Borschneck, D., Bottero, J. Y., Moustier, S., Masin, F., and Colin, F.: Mineral control of carbon pools in a volcanic soil horizon, Geoderma, 137, 477-489, http://dx.doi.org/10.1016/j.geoderma.2006.10.006, 2007.

Basile-Doelsch, I., Brun, T., Borschneck, D., Masion, A., Marol, C., and Balesdent, J.: Effect of landuse on organic matter stabilized in organomineral complexes: A study combining density fractionation, mineralogy and δ13C, Geoderma, 151, 550 77-86, http://dx.doi.org/10.1016/j.geoderma.2009.03.008, 2009.

Blankinship, J. C., Berhe, A. A., Crow, S. E., Druhan, J. L., Heckman, K. A., Keiluweit, M., Lawrence, C. R., Marín-Spiotta, E., Plante, A. F., Rasmussen, C., Schädel, C., Schimel, J. P., Sierra, C. A., Thompson, A., Wagai, R., and Wieder, W. R.: Improving understanding of soil organic matter dynamics by triangulating theories, measurements, and models, Biogeochemistry, 140, 1-13, 10.1007/s10533-018-0478-2, 2018.

555 Chen, C., Dynes, J. J., Wang, J., and Sparks, D. L.: Properties of Fe-Organic Matter Associations via Coprecipitation versus Adsorption, Environmental Science & Technology, 48, 13751-13759, 10.1021/es503669u, 2014.

Chen, C., Hall, S. J., Coward, E., and Thompson, A.: Iron-mediated organic matter decomposition in humid soils can counteract protection, Nature Communications, 11, 2255, 10.1038/s41467-020-16071-5, 2020.

Christensen, B. T.: Physical fractionation of soil and structural and functional complexity in organic matter turnover, Eur. J. 560 Soil Sci., 52, 345-353, 10.1046/j.1365-2389.2001.00417.x, 2001.

Churchman, G. J., and Tate, K. R.: Aggregation of clay in six New Zealand soil types as measured by disaggregation procedures, Geoderma, 37, 207-220, https://doi.org/10.1016/0016-7061(86)90049-2, 1986.

Coleman, K., and Jenkinson, D. S.: RothC-26.3 - A Model for the turnover of carbon in soil, in: Evaluation of Soil Organic Matter Models, edited by: D.S., P., P., S., and J.U., S., Springer, Berlin, Heidelberg, 1996.

565 Cornell, R. M., and Schwertmann, U.: The Iron Oxides: Structure, Properties, Reactions, Occurences and Uses, 2nd ed., Wiley-VCH, 664 pp., 2003.

Coward, E. K., Thompson, A. T., and Plante, A. F.: Iron-mediated mineralogical control of organic matter accumulation in tropical soils, Geoderma, 306, 206-216, https://doi.org/10.1016/j.geoderma.2017.07.026, 2017.

Coward, E. K., Thompson, A., and Plante, A. F.: Contrasting Fe speciation in two humid forest soils: Insight into organomineral 570 associations in redox-active environments, Geochimica et Cosmochimica Acta, 238, 68-84, https://doi.org/10.1016/j.gca.2018.07.007, 2018.

Crow, S., Reeves, M., Schubert, O., and Sierra, C.: Optimization of method to quantify soil organic matter dynamics and carbon sequestration potential in volcanic ash soils, Biogeochemistry, 1-21, 10.1007/s10533-014-0051-6, 2014.

Dahlgren, R., Shoji, S., and Nanzyo, M.: Mineralogical characteristics of volcanic ash soils, in: Volcanic Ash Soils: genesis, 575 properties, and utilization, edited by: Shoji, S., Nanzyo, M., and Dahlgren, R., Elsevier, 101-143, 1993.

Dai, Q.-x., Ae, N., Suzuki, T., Rajkumar, M., Fukunaga, S., and Fujitake, N.: Assessment of potentially reactive pools of aluminum in Andisols using a five-step sequential extraction procedure, Soil Sci Plant Nutr, 57, 500-507, 10.1080/00380768.2011.598445, 2011.

Drees, R. L., Wilding, L., Smeck, N., and Senkayi, A.: Silica in soils: quartz and disordered silica polymorphs, in: Minerals in
580    Soil Environments, 2nd ed., edited by: Dixon, J. B., Weed, S.B., Soil Science Society of America Book Series, Soil Science Society of America, 913-974, 1989.

Dultz, S., Woche, S. K., Mikutta, R., Schrapel, M., and Guggenberger, G.: Size and charge constraints in microaggregation: Model experiments with mineral particle size fractions, Applied Clay Science, 170, 29-40, https://doi.org/10.1016/j.clay.2019.01.002, 2019.

585    Eusterhues, K., Rumpel, C., Kleber, M., and Kögel-Knabner, I.: Stabilisation of soil organic matter by interactions with minerals as revealed by mineral dissolution and oxidative degradation, Organic Geochemistry, 34, 1591-1600, https://doi.org/10.1016/j.orggeochem.2003.08.007, 2003.

Ferris, F. G., Tazaki, K., and Fyfe, W. S.: Iron oxides in acid mine drainage environments and their association with bacteria, Chem Geol, 74, 321-330, https://doi.org/10.1016/0009-2541(89)90041-7, 1989.

590    Filimonova, S., Kaufhold, S., Wagner, F. E., Häusler, W., and Kögel-Knabner, I.: The role of allophane nano-structure and Fe oxide speciation for hosting soil organic matter in an allophanic Andosol, Geochimica et Cosmochimica Acta, 180, 284-302, https://doi.org/10.1016/j.gca.2016.02.033, 2016.

Fujii, K., Hayakawa, C., Inagaki, Y., and Ono, K.: Sorption reduces the biodegradation rates of multivalent organic acids in volcanic soils rich in short-range order minerals, Geoderma 333: 188-199, 2019.

595    Garcia Arredondo, M., Lawrence, C. R., Schulz, M. S., Tfaily, M. M., Kukkadapu, R., Jones, M. E., Boye, K., and Keiluweit, M.: Root-driven weathering impacts on mineral-organic associations in deep soils over pedogenic time scales, Geochimica et Cosmochimica Acta, 263, 68-84, https://doi.org/10.1016/j.gca.2019.07.030, 2019.

Gunina, A., and Kuzyakov, Y.: Pathways of litter C by formation of aggregates and SOM density fractions: Implications from 13C natural abundance, Soil Biology and Biochemistry, 71, 95-104, http://dx.doi.org/10.1016/j.soilbio.2014.01.011,
600    2014.

Hatton, P.-J., Kleber, M., Zeller, B., Moni, C., Plante, A. F., Townsend, K., Gelhaye, L., Lajtha, K., and Derrien, D.: Transfer of litter-derived N to soil mineral–organic associations: Evidence from decadal 15N tracer experiments, Organic Geochemistry, 42, 1489-1501, https://doi.org/10.1016/j.orggeochem.2011.05.002, 2012.

Heckman, K., Grandy, A. S., Gao, X., Keiluweit, M., Wickings, K., Carpenter, K., Chorover, J., and Rasmussen, C.: Sorptive
605    fractionation of organic matter and formation of organo-hydroxy-aluminum complexes during litter biodegradation in the presence of gibbsite, Geochimica et Cosmochimica Acta, 121, 667-683, https://doi.org/10.1016/j.gca.2013.07.043, 2013.

Heckman, K., Lawrence, C. R., and Harden, J. W.: A sequential selective dissolution method to quantify storage and stability of organic carbon associated with Al and Fe hydroxide phases, Geoderma, 312, 24-35,
610    https://doi.org/10.1016/j.geoderma.2017.09.043, 2018.

Inagaki, T. M., Possinger, A. R., Grant, K. E., Schweizer, S. A., Mueller, C. W., Derry, L. A., Lehmann, J., and Kögel-Knabner, I.: Subsoil organo-mineral associations under contrasting climate conditions, Geochimica et Cosmochimica Acta, 270, 244-263, https://doi.org/10.1016/j.gca.2019.11.030, 2020.

Jones, E., and Singh, B.: Organo-mineral interactions in contrasting soils under natural vegetation, Frontiers in Environmental Science, 2, 10.3389/fenvs.2014.00002, 2014.

Kaiser, K., and Zech, W.: Defects in Estimation of Aluminum in Humus Complexes of Podzolic Soils By Pyrophosphate Extraction, Soil Science, 161, 452-458, 1996.

Kaiser, K.: Sorption of natural organic matter fractions to goethite (α-FeOOH): effect of chemical composition as revealed by liquid-state 13C NMR and wet-chemical analysis, Organic Geochemistry, 34, 1569-1579, https://doi.org/10.1016/S0146-6380(03)00120-7, 2003.

Kaiser, K., and Guggenberger, G.: Mineral surfaces and soil organic matter, Eur. J. Soil Sci., 54, 219-236, 10.1046/j.1365-2389.2003.00544.x, 2003.

Kaiser, K., and Guggenberger, G.: Distribution of hydrous aluminium and iron over density fractions depends on organic matter load and ultrasonic dispersion, Geoderma, 140, 140-146, 10.1016/j.geoderma.2007.03.018, 2007.

Keil, R. G., and Mayer, L. M.: 12.12 - Mineral Matrices and Organic Matter, in: Treatise on Geochemistry (Second Edition), edited by: Holland, H. D., and Turekian, K. K., Elsevier, Oxford, 337-359, 2014.

Keiluweit, M., Bougoure, J. J., Nico, P. S., Pett-Ridge, J., Weber, P. K., and Kleber, M.: Mineral protection of soil carbon counteracted by root exudates, Nature Climate Change, 5, 588-595, 10.1038/nclimate2580, 2015.

Kleber, M., Sollins, P., and Sutton, R.: A conceptual model of organo-mineral interactions in soils: self-assembly of organic molecular fragments into zonal structures on mineral surfaces, Biogeochemistry, 85, 9-24, 10.1007/s10533-007-9103-5, 2007.

Kleber, M., Eusterhues, K., Keiluweit, M., Mikutta, C., Mikutta, R., and Nico, P. S.: Mineral–Organic Associations: Formation, Properties, and Relevance in Soil Environments, in: Advances in Agronomy, edited by: Donald, L. S., Advances in Agronomy, Academic Press, 1-140, 2015.

Kramer, M. G., Sanderman, J., Chadwick, O. A., Chorover, J., and Vitousek, P. M.: Long-term carbon storage through retention of dissolved aromatic acids by reactive particles in soil, Global Change Biology, 18, 2594-2605, 10.1111/j.1365-2486.2012.02681.x, 2012.

Kramer, M. G., and Chadwick, O. A.: Climate-driven thresholds in reactive mineral retention of soil carbon at the global scale, Nature Climate Change, 8, 1104-1108, 10.1038/s41558-018-0341-4, 2018.

Lalonde, K., Mucci, A., Ouellet, A., and Gelinas, Y.: Preservation of organic matter in sediments promoted by iron, Nature, 483, 198-200, 10.1038/nature10855, 2012.

Lavallee, J. M., Soong, J. L., and Cotrufo, M. F.: Conceptualizing soil organic matter into particulate and mineral-associated forms to address global change in the 21st century, Global Change Biology, n/a, 10.1111/gcb.14859, 2020.

Lawrence, C. R., Harden, J. W., Xu, X., Schulz, M. S., and Trumbore, S. E.: Long-term controls on soil organic carbon with depth and time: A case study from the Cowlitz River Chronosequence, WA USA, Geoderma, 247–248, 73-87, http://dx.doi.org/10.1016/j.geoderma.2015.02.005, 2015.

Lehmann, J., Kinyangi, J., and Solomon, D.: Organic matter stabilization in soil microaggregates: implications from spatial heterogeneity of organic carbon contents and carbon forms, Biogeochemistry, 85, 45-57, 10.1007/s10533-007-9105-3, 2007.

Lehmann, J., and Kleber, M.: The contentious nature of soil organic matter, Nature, 528, 60-68, 10.1038/nature16069, 2015.

Loeppert, R. H., and Inskeep, W. P.: Iron, in: Methods of Soil Analysis, edited by: Sparks, D. L., Soil Sci. Soc. Am., Madison, WI, 639-664, 1996.

Lundström, U. S., van Breemen, N., and Bain, D.: The podzolization process. A review, Geoderma, 94, 91-107, https://doi.org/10.1016/S0016-7061(99)00036-1, 2000.

Masiello, C. A., Chadwick, O. A., Southon, J., Torn, M. S., and Harden, J. W.: Weathering controls on mechanisms of carbon storage in grassland soils, Global Biogeochem. Cycles, 18, GB4023, 10.1029/2004gb002219, 2004.

Mayer, L. M., and Xing, B.: Organic Matter–Surface Area Relationships in Acid Soils, Soil Science Society of America Journal, 65, 250-258, 10.2136/sssaj2001.651250x, 2001.

Mayer, L. M., Schick, L. L., Hardy, K. R., Wagai, R., and McCarthy, J.: Organic matter in small mesopores in sediments and soils, Geochimica et Cosmochimica Acta, 68, 3863-3872, 10.1016/j.gca.2004.03.019, 2004.

Mikutta, R., Kleber, M., Torn, M. S., and Jahn, R.: Stabilization of Soil Organic Matter: Association with Minerals or Chemical Recalcitrance?, Biogeochemistry, 77, 25-56, 2006.

Mikutta, R., Zang, U., Chorover, J., Haumaier, L., and Kalbitz, K.: Stabilization of extracellular polymeric substances (Bacillus subtilis) by adsorption to and coprecipitation with Al forms, Geochimica et Cosmochimica Acta, 75, 3135-3154, https://doi.org/10.1016/j.gca.2011.03.006, 2011.

Nierop, K. G. J. J., Jansen, B., and Verstraten, J. M.: Dissolved organic matter, aluminium and iron interactions: precipitation induced by metal/carbon ratio, pH and competition, Science of The Total Environment, 300, 201-211, https://doi.org/10.1016/S0048-9697(02)00254-1, 2002.

Oades, J. M., and Waters, A. G.: Aggregate Hierarchy in Soils, Aust. J. Soil Res., 29, 815-828, 1991.

Parfitt, R. L.: Allophane and imogolite: role in soil biogeochemical processes, Clay Minerals, 44, 135-155, 10.1180/claymin.2009.044.1.135, 2009.

Parton, W. J., Schimel, D. S., Cole, C. V., and Ojima, D. S.: Analysis of Factors Controlling Soil Organic Matter Levels in Great Plains Grasslands, Soil Science Society of America Journal, 51, 1173-1179, 10.2136/sssaj1987.03615995005100050015x, 1987.

Percival, H. J., Parfitt, R. L., and Scott, N. A.: Factors Controlling Soil Carbon Levels in New Zealand Grasslands Is Clay Content Important?, Soil Sci. Soc. Am. J., 64, 1623-1630, 10.2136/sssaj2000.6451623x, 2000.

Porras, R. C., Hicks Pries, C. E., McFarlane, K. J., Hanson, P. J., and Torn, M. S.: Association with pedogenic iron and aluminum: effects on soil organic carbon storage and stability in four temperate forest soils, Biogeochemistry, 133, 333-345, 10.1007/s10533-017-0337-6, 2017.

680 Rasmussen, C., Heckman, K., Wieder, W. R., Keiluweit, M., Lawrence, C. R., Berhe, A. A., Blankinship, J. C., Crow, S. E., Druhan, J. L., Hicks Pries, C. E., Marin-Spiotta, E., Plante, A. F., Schädel, C., Schimel, J. P., Sierra, C. A., Thompson, A., and Wagai, R.: Beyond clay: towards an improved set of variables for predicting soil organic matter content, Biogeochemistry, 137, 297-306, 10.1007/s10533-018-0424-3, 2018.

Rennert, T.: Wet-chemical extractions to characterise pedogenic Al and Fe species – a critical review, Soil Research, 57, 1-16, https://doi.org/10.1071/SR18299, 2019.

685

Schneider, M. P. W., Scheel, T., Mikutta, R., van Hees, P., Kaiser, K., and Kalbitz, K.: Sorptive stabilization of organic matter by amorphous Al hydroxide, Geochimica et Cosmochimica Acta, 74, 1606-1619, 10.1016/j.gca.2009.12.017, 2010.

Schuppli, P. A., Ross, G. J., and McKeague, J. A.: The effective removal of suspended materials from pyrophosphate extracts of soils from tropical and temperate regions, Soil Science Society of America Journal, 47, 1026-1032, 690 10.2136/sssaj1983.03615995004700050037x, 1983.

Shang, C., and Tiessen, H.: Organic matter stabilization in two semiarid tropical soils: Size, density, and magnetic separations, Soil Science Society of America Journal, 62, 1247-1257, 1998.

Shoji, S., Nanzyo, M., and Dahlgren, R.: Volcanic Ash Soils: genesis, properties, and utilization, Developments in Soil Science: 21, Elsevier, Amsterdam, 288 pp., 1993.

695 Six, J., Merckx, R., Kimpe, K., Paustian, K., and Elliott, E. T.: A re-evaluation of the enriched labile soil organic matter fraction, Eur. J. Soil Sci., 51, 283-293, 10.1046/j.1365-2389.2000.00304.x, 2000.

Six, J., Conant, R. T., Paul, E. A., and Paustian, K.: Stabilization mechanisms of soil organic matter: Implications for C-saturation of soils, Plant and Soil, 241, 155-176, 10.1023/A:1016125726789, 2002.

Smith, P.: Soil carbon sequestration and biochar as negative emission technologies, Global Change Biology, 22, 1315-1324, 700 10.1111/gcb.13178, 2016.

Sollins, P., Homann, P., and Caldwell, B. A.: Stabilization and destabilization of soil organic matter: mechanisms and controls, Geoderma, 74, 65-105, 10.1016/s0016-7061(96)00036-5, 1996.

Sollins, P., Glassman, C., Paul, E. A., Swanston, C., Lajtha, K., Heil, W., and Elliott, E. T.: Soil carbon and nitrogen: pools and fractions, in: Standard Soil Methods for Long-Term Ecological Research, edited by: Robertson, P., Coleman, D. C., 705 Bledsoe, C. S., and Sollins, P., Oxford University Press, Oxford, 89-105, 1999.

Sollins, P., Kramer, M., Swanston, C., Lajtha, K., Filley, T., Aufdenkampe, A., Wagai, R., and Bowden, R.: Sequential density fractionation across soils of contrasting mineralogy: evidence for both microbial- and mineral-controlled soil organic matter stabilization, Biogeochemistry, 96, 209-231, 10.1007/s10533-009-9359-z, 2009.

Suda, A., and Makino, T.: Functional effects of manganese and iron oxides on the dynamics of trace elements in soils with a 710 special focus on arsenic and cadmium: A review, Geoderma, 270, 68-75, http://dx.doi.org/10.1016/j.geoderma.2015.12.017, 2016.

Takahashi, T., and Dahlgren, R. A.: Nature, properties and function of aluminum–humus complexes in volcanic soils, Geoderma, 263, 110-121, http://dx.doi.org/10.1016/j.geoderma.2015.08.032, 2016.

Tamrat, W. Z., Rose, J., Grauby, O., Doelsch, E., Levard, C., Chaurand, P., and Basile-Doelsch, I.: Soil organo-mineral associations formed by co-precipitation of Fe, Si and Al in presence of organic ligands, Geochimica et Cosmochimica Acta, 260, 15-28, https://doi.org/10.1016/j.gca.2019.05.043, 2019.

Torn, M. S., Trumbore, S. E., Chadwick, O. A., Vitousek, P. M., and Hendricks, D. M.: Mineral control of soil organic carbon storage and turnover, Nature, 389, 170-173, 1997.

Totsche, K. U., Amelung, W., Gerzabek, M. H., Guggenberger, G., Klumpp, E., Knief, C., Lehndorff, E., Mikutta, R., Peth, S., Prechtel, A., Ray, N., and Kögel-Knabner, I.: Microaggregates in soils, Journal of Plant Nutrition and Soil Science, 10.1002/jpln.201600451, 2017.

Turchenek, L. W., and Oades, J. M.: Fractionation of organo-mineral complexes by sedimentation and density techniques, Geoderma, 21, 311-343, 1979.

Urrutia, M. M., and Beveridge, T. J.: Formation of fine-grained metal and silicate precipitates on a bacterial surface (Bacillus subtilis), Chem Geol, 116, 261-280, https://doi.org/10.1016/0009-2541(94)90018-3, 1994.

von Lützow, M., Kögel-Knabner, I., Ekschmitt, K., Flessa, H., Guggenberger, G., Matzner, E., and Marschner, B.: SOM fractionation methods: Relevance to functional pools and to stabilization mechanisms, Soil Biology and Biochemistry, 39, 2183-2207, DOI: 10.1016/j.soilbio.2007.03.007, 2007.

Wada, K., and Higashi, T.: The categories of aluminum- and iron-humus complexes in ando soils determined by selective dissolution, Journal of Soil Science, 27, 357-368, 10.1111/j.1365-2389.1976.tb02007.x, 1976.

Wada, K., and Kakuto, Y.: Intergradient vermiculite-kaolin mineral in a Korean Ultisol, Clays and Clay Minerals, 31, 183-190, 1983.

Wada, K.: Allophane and Imogolite, in: Minerals in Soil Environments, 1051-1087, 2018.

Wagai, R., and Mayer, L. M.: Sorptive stabilization of organic matter in soils by hydrous iron oxides, Geochimica Et Cosmochimica Acta, 71, 25-35, 10.1016/j.gca.2006.08.047, 2007.

Wagai, R., Mayer, L. M., Kitayama, K., and Shirato, Y.: Association of organic matter with iron and aluminum across a range of soils determined via selective dissolution techniques coupled with dissolved nitrogen analysis, Biogeochemistry, 112, 95-109, 10.1007/s10533-011-9652-5, 2013.

Wagai, R., Kajiura, M., Asano, M., and Hiradate, S.: Nature of soil organo-mineral assemblage examined by sequential density fractionation with and without sonication: Is allophanic soil different?, Geoderma, 241–242, 295-305, http://dx.doi.org/10.1016/j.geoderma.2014.11.028, 2015.

Wagai, R., Kajiura, M., Uchida, M., and Asano, M.: Distinctive roles of two aggregate binding agents in allophanic andisols: young carbon and poorly-crystalline metal phases with old carbon, Soil Systems, 2, 29, 2018.

Wan, J., Tyliszczak, T., and Tokunaga, T. K.: Organic carbon distribution, speciation, and elemental correlations within soil microaggregates: Applications of STXM and NEXAFS spectroscopy, Geochimica et Cosmochimica Acta, 71, 5439-5449, 10.1016/j.gca.2007.07.030, 2007.

23

Wen, Y., Li, H., Xiao, J., Wang, C., Shen, Q., Ran, W., He, X., Zhou, Q., and Yu, G.: Insights into complexation of dissolved organic matter and Al(III) and nanominerals formation in soils under contrasting fertilizations using two-dimensional correlation spectroscopy and high resolution-transmission electron microscopy techniques, Chemosphere, 111, 441-449, https://doi.org/10.1016/j.chemosphere.2014.03.078, 2014.

Wieder, W. R., Grandy, A. S., Kallenbach, C. M., Taylor, P. G., and Bonan, G. B.: Representing life in the Earth system with soil microbial functional traits in the MIMICS model, Geosci. Model Dev., 8, 1789-1808, 10.5194/gmd-8-1789-2015, 2015.

Yang, J., Liu, J., Hu, Y., Rumpel, C., Bolan, N., and Sparks, D.: Molecular-level understanding of malic acid retention mechanisms in ternary kaolinite-Fe(III)-malic acid systems: The importance of Fe speciation, Chem Geol, 464, 69-75, https://doi.org/10.1016/j.chemgeo.2017.02.018, 2017.

Yu, G.: Root Exudates and Microbial Communities Drive Mineral Dissolution and the Formation of Nano-size Minerals in Soils: Implications for Soil Carbon Storage, in: Root Biology, edited by: Giri, B., Prasad, R., and Varma, A., Springer International Publishing, Cham, 143-166, 2018.

Zhao, Q., Poulson, S. R., Obrist, D., Sumaila, S., Dynes, J. J., McBeth, J. M., and Yang, Y.: Iron-bound organic carbon in forest soils: quantification and characterization, Biogeosciences, 13, 4777-4788, 10.5194/bg-13-4777-2016, 2016.
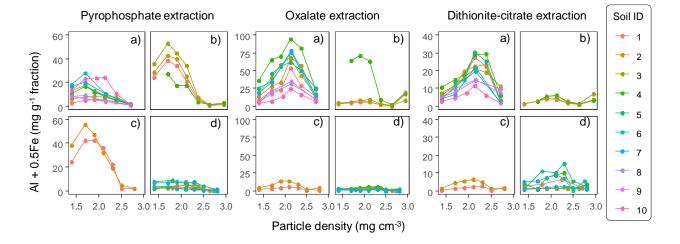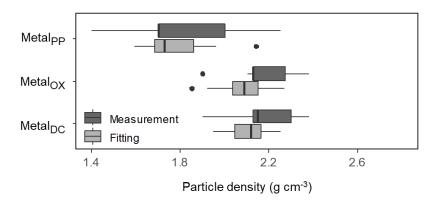
**Figures**

765



**Figure 1: The concentrations of pedogenic metal (Al+0.5Fe) per fraction along the density gradient for allophanic Andisol group (a), non-allophanic Andisol group (b), Spodosol group (c) and crystalline mineral group (d). The metal extracted by initial pyrophosphate (left panels), subsequent acid oxalate (central panels), and final dithionite-citrate reagents (right panels) are**
770 **shown. Each symbol represents individual soil sample. Sample number (1-10) on the right corresponds to sample ID for each soil group in Table 1.**



775 **Figure 2: Boxplot showing the median and variation of densities at which the concentration of pedogenic metal (Al+0.5Fe) was the highest across the 23 studied soils. The peak density was determined for all three extractions (PP, OX, and DC) for each soil based on measurements (light color) and normal distribution fitting (dark color).**

780



**Figure 3: Scatter plot of extractable metals and co-dissolved organic C (DOC) for the density fractions from the studied soils.**
785 **Pyrophosphate-extractable Al (a), Fe (b), and Al+0.5Fe (c) against DOC$_{OX}$ in upper panel. Oxalate-extractable Al (d), Fe (e), and Al+0.5Fe (f) against DOC$_{OX}$ in lower panel. Symbol color distinguishes the four soil groups and its shape corresponds to sample ID in Table 1.**
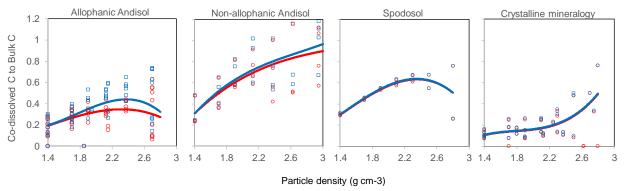
790

795

**Figure 4: Proportions of bulk C in each density fraction co-dissolved by initial pyrophosphate extraction alone (red circle) and combined with subsequent acid oxalate extraction (blue rectangle), with polynomial fitting curves, for each soil group.**



**Figure 5: Boxplot showing the median and distribution of the densities at which the distribution of mass, C, and pedogenic metal (Al+0.5Fe) extracted by the three extractants (PP, OX, and DC) were the highest among the 23 studied soils.**
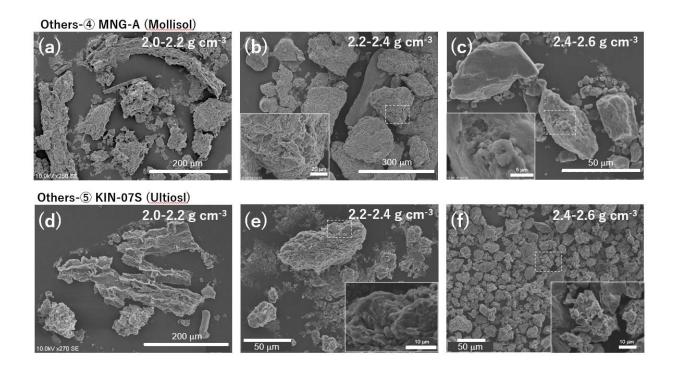
815

**Figure 6: SEM images of three meso-density fractions from two selected soils. Dotted rectangular section is enlarged in a bottom corner for (b,e,f) to show aggregated nature of selected particles and clay coating (c).**
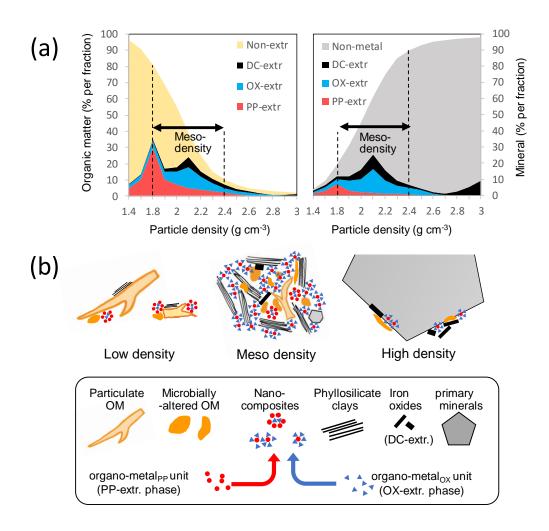
820

825

**Figure 7: (a) Changes in the concentration of organic and mineral phases along soil particle gradient for an idealized soil. The concentrations of OM (left plot) and metals (right plot) extracted sequentially by pyrophosphate (PP), acid oxalate (OX), and dithionite (DC) per density fraction were shown in different colors. Non-extractable OM includes both particulate and microbially-altered OM. Non-metal mineral phase includes phyllosilicate clays and primary minerals. (b) Schematic representation of low-, meso-, and high-density particles (upper) and their building blocks (lower). PP- and OX-extractable phases were presumed to be present as "nanocomposites" that act as glue to form meso-density microaggregates. The distribution of the nanocomposites across density fractions can explain the C:metal proportional relationship found in Fig. 3, A5, and A6. The nanocomposites rich in organo-metal$_{PP}$ unit is more abundant in OM-rich environments (e.g., lower-density fraction) relative to those rich in organo-metal$_{OX}$ units. Objects don't reflect the size difference among them.**
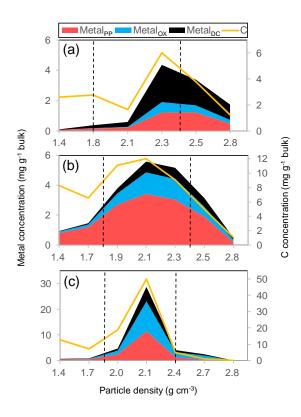
845



**Figure 8: The distribution of the extractable metal phases (Al+0.5Fe) on left Y axis and that of C on the right Y axis along the density gradient for three undisturbed forest soils. A kaolinitic Ultisol (O-5 in Table 1) developed from sedimentary rock under tropical wet climate (a), a Spodosol Bhs horizon (S-2) with quartz and plagioclase rich mineralogy from glacial till under cool temperate moist climate (b), and an allophanic Andisol (A-10) from tephra under warm temperate moist climate (c). Vertical**
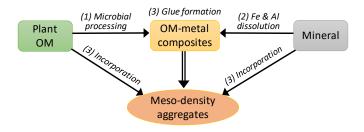850 **dotted lines show the meso-density range.**



**Figure 9: Conceptual illustration of meso-density aggregate formation. Three main processes are (1) microbial processing of**
855 **plant-derived organic matter, (2) metal dissolution via chemical weathering, and (3) the formation of organo-metallic glue which promote meso-density microaggregate formation by incorporating some of POM and mineral.**

SOIL
Discussions
Open Access
EGU

## Tables

**Table 1. Sample source information and basic soil characteristics**

Table 1. Sample source information and basic soil characteristics.

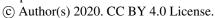| Sample ID | Site | Climate zone [a, b] | MAT °C | MAP mm yr^{-1} | Soil order [c] | Landuse [a] | Vegetation/Management | Horizon /depth (cm) | TOC mg g^{-1} | TN mg g^{-1} | Soil pH (H$_2$O) | Clay (%) |
|---|---|---|---|---|---|---|---|---|---|---|---|---|
| *Andisols, allophanic* | | | | | | | | | | | | |
| A-1[d] / NIAES-NTa | Tsukuba, Japan | WTM | 13.7 | 1300 | Andisol | cropland | no-till with leaf compost | Ap/ 0-5 | 149 | 10 | 6.2 | 45-55 |
| A-2[d] / NIAES-NTb | | | | | | | | Ap/ 5-20 | 80.4 | 5.9 | 6.2 | 45-55 |
| A-3[d] / NIAES-Till1 | | | | | | | till + NPK | Ap/ 0-20 | 51.4 | 4.1 | 6.1 | 45-55 |
| A-4[d] / NIAES-Till2 | | | | | | | till (stump removed) | Ap/ 0-20 | 42.3 | 3.6 | 6.7 | 45-55 |
| A-5 / NIAES-Bare | | | | | | | bare fallow | Ap/ 0-20 | 36.9 | 3.0 | 6.5 | 45-55 |
| A-6 / TKY-NPK | Tokyo, Japan | WTM | 14.7 | 1515 | Andisol | cropland | till + NPK | Ap/ 0-14 | 46.5 | 3.9 | 4.1 | 27 |
| A-7 / TKY-comp | | | | | | | till + NPK + compost | Ap/ 0-14 | 60.3 | 5.4 | 5.0 | 28 |
| A-8 / YMS-NPK | Yamanashi, Japan | WTM | 12.1 | 1137 | Andisol | cropland | till + NPK | Ap/ 0-14 | 29.1 | 2.8 | 6.6 | 28 |
| A-9 / YMS-straw | | | | | | | till + NPK + rice straw | Ap/ 0-14 | 35.5 | 3.2 | 6.7 | 28 |
| A-10 / MtTKB-A | Tsukuba, Japan | WTM | ∣13.1 | 1438 | Andisol | forest | secondary forest (mixed) | A/ 0-15 | 97.7 | 7.6 | 4.6 | 35-45 |
| *Andisols, non-allophanic* | | | | | | | | | | | | |
| N-1[e] / KWT-A1 | Kawatabi, Japan | WTM | 10.1 | 1460 | Andisol | grassland | semi-managed | A1/ 0-25 | 105 | 6.7 | 4.6 | 23 |
| N-2[e] / KWT-A2 | | | | | | | | A2/ 25-52 | 102 | 5.6 | 4.6 | 18 |
| N-3[e] / KWT-2A3 | | | | | | | | 2A3/ 52-100 | 98.3 | 4.9 | 4.9 | 25 |
| N-4[e] / KWT-3Bw | | | | | | | | 3Bw/ 120-140 | 12.1 | 0.9 | 5.2 | 11 |
| *Spodosols* | | | | | | | | | | | | |
| S-1 / MBB-CN | Maine, USA | CTM | ~5 | 1365 | Spodosol | forest | conifer (red spruce) | Bhs/ 5-15 | 146 | 5.8 | 3.7 | 18-35 |
| S-2 / MBB-DD | | | | | | forest | mixed hardwood | Bhs/ 7-22 | 58.9 | 2.4 | 4.6 | 18-35 |
| *Crystalline mineralogy soils* | | | | | | | | | | | | |
| C-1 / NGK-straw | Aichi, Japan | WTM | 14.9 | 1447 | Inceptisol | cropland | rice paddy + manure | Ap/ 0-15 | 24.1 | 2.1 | 5.9 | |
| C-2 / WKY-NPK | Wakayama, Japan | WTM | 15.3 | 1286 | Ultisol | cropland | till + NPK | Ap/ 0-16 | 9.8 | 1.0 | 5.8 | 15-25 |
| C-3 / WKY-straw | | | | | | cropland | till + NPK + manure | Ap/ 0-16 | 28.8 | 2.5 | 6.4 | 15-25 |
| C-4 / MNG-A | NE Mongolia | CTD | ND | 221 | Mollisol | grassland | forest steppe | A1/ 0-10 | 24.2 | 2.5 | 6.3-7.2 | 15-25 |
| C-5 / KIN-07S | Saba, Malaysia | TW | 24.0 | 2392 | Ultisol | forest | tropical (hill dipterocarp) | A/ 0-10 | 20.9 | 1.9 | 3.9 | 33-38 |
| C-6 / KIN-17S | Saba, Malaysia | TM | 19.0 | 2380 | Inceptisol | forest | tropical (lower montane) | A/ 0-10 | 42.0 | 2.5 | 4.1 | 10-13 |
| C-7 / KIN-27S | Saba, Malaysia | WTM | 13.0 | 2256 | Inceptisol | forest | tropical (upper montane) | A/ 0-10 | 125 | 8.4 | 3.9 | 6-15 |

[a] Based on 2006 IPCC Guidelines for National Greenhouse Gas Inventories. Vol. 4. Chapter 3: Consistent Representation of Lands.

[b] Climate zones. WTM: warm temperate moist, CTM: cool temperate moist, CTD: cool temperate dry, TW: tropical wet, and TM: tropical montane.

[c] Soil taxonomy, USDA, soil survey staff.

[d] Data from Wagai et al. (2018). A well-studied allophanic Andisol at the experimental field of NIAES/NARO, developed on andesitic and basaltic volcanic ashes.

[e] N1-N4: Kawatabi Andisol (Pacllic Mdanudand) is a typical, non-allophanic Andisol at Kawatabi Field Science Center of Tohoku University, Miyagi, Japan, located on a gentle slope of a fan in mountain valleys at 190 m elevation under native grassland (Sasa nipponica). Parent material is dacitic volcanic tephra with alluvium including smectitic sedimentary rock.
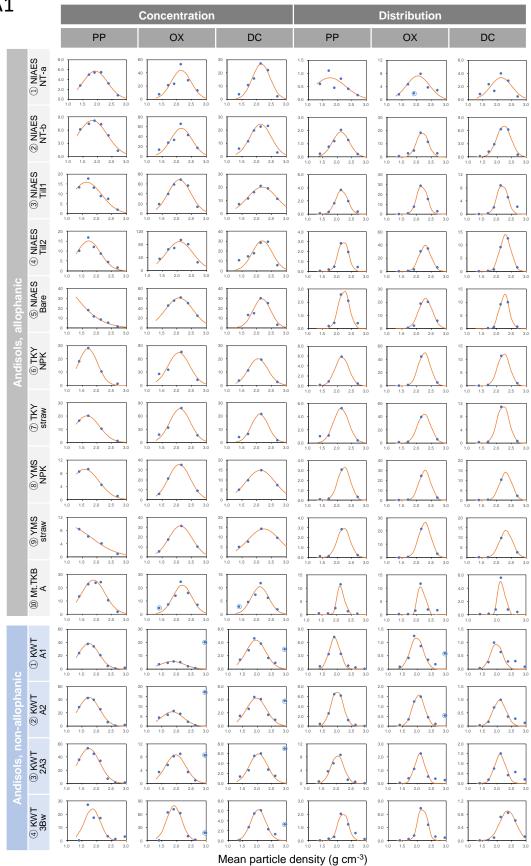
860

SOIL Discussions
Open Access
EGU

865 **Table 2. Recoveries of mass, C, N, and the metals dissolved by initial pyrophosphate (PP) and subsequent acid oxalate (OX) and dithionite-citrate (DC) extractions from the density fractions, expressed as percentage relative to the whole soil. Values show means (standard deviations) of all soils and separately for Andisols (allophanic and non-allophanic Andisols) and non-Andisols (Spodosols and crystalline mineral soils).**

| Soil group | Mass | C | N | PP extr. Al+0.5Fe | OX extr. Al+0.5Fe | DC extr. Al+0.5Fe | Sum of PP, OX, and DC extractions | | |
|---|---|---|---|---|---|---|---|---|---|
| | | | | | | | Al | Fe | Si |
| All soils (n=23) | 99.8 (2.9) | 97.5 (9.5) | 95.6 (10.6) | 104.6 (33.3) | 98.8 (20.5) | 86.4 (16.9) | 88.8 (16.0) | 94.4 (11.2) | 93.6 (20.4) |
| Non-Andisols (n=9) | 96.8 (2.1) | 90.3 (8.9) | 86.8 (8.9) | 83.9 (12.0) | 89.4 (12.5) | 86.7 (15.5) | 78.7 (15.0) | 86.7 (12.0) | 80.8 (9.3) |
| Andisols (n=14) | 101.3 (1.9) | 102.2 (6.7) | 101.3 (7.4) | 117.9 (36.0) | 104.9 (22.7) | 86.3 (18.4) | 95.4 (13.4) | 99.3 (7.5) | 101.9 (21.5) |

## Figure A1
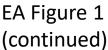


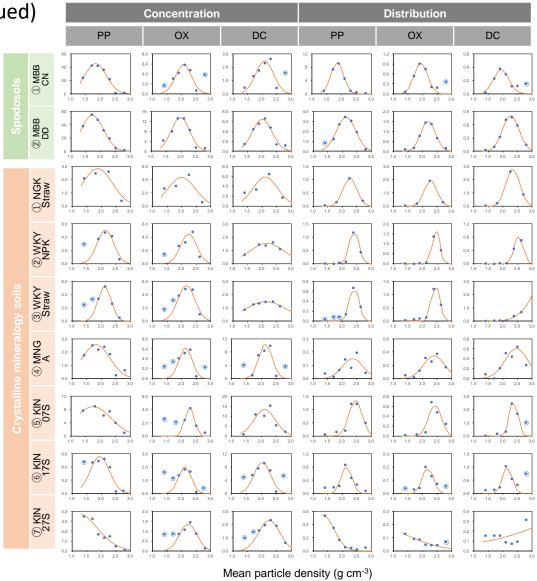Mean particle density (g cm⁻³)

# EA Figure 1 (continued)



Figure A1. Extractable metal (Al+0.5Fe) against mean particle density for each soil sample. The metal concentrations (mg g⁻¹ fraction) from pyrophosphate (PP), acid oxalate (OX), and dithionite-citrate (DC) extractions are shown in the left three panels. The distributions of PP, OX, DC-extractable metal phases (mg g⁻¹ whole soil) are in the right three panels. Normal distribution curve fit is shown as line. The data points circled in blue were omitted from the fitting.

# Fig. A2



Figure A2. Boxplot of r squared value for the normal distribution curve fitting of the extractable metal concentration (a) and distribution (b) against mean particle density. The fitting was done for each soil and each extraction as shown in EA. Fig. 1.
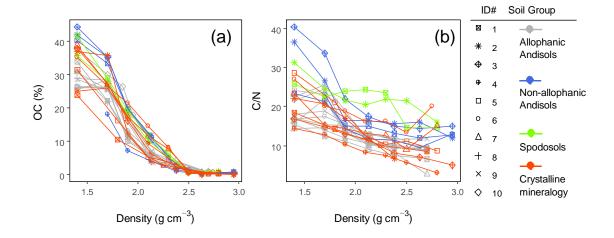
# Fig. A3



Figure A3. Line graphs showing organic C concentration (a) and C:N ratio (b) against soil particle density. Four soil groups were shown in different colors with the ID number (corresponding to Table 1) in different symbol shapes.
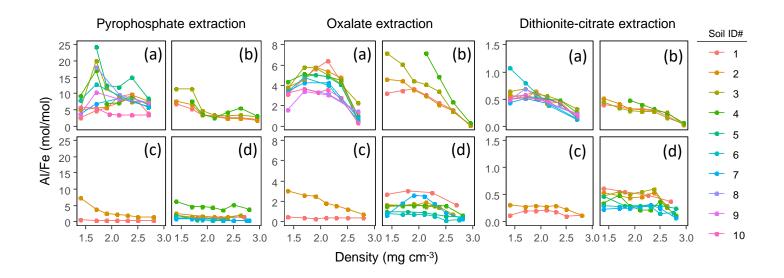
# Fig. A4



Figure A4. Molar Al-to-Fe ratio of each extractable phase from each density fraction along the density gradient. The ratio was shown for initial pyrophosphate (left four plots), subsequent acid oxalate (middle four plots), and final dithionite-citrate extractions (right four plots) were shown for Allophanic Andisols (a), non-allophanic Andisols (b), Spodosols (c), and crystalline mineralogy group (d). Each symbol represents individual soil sample ID in Table 1.
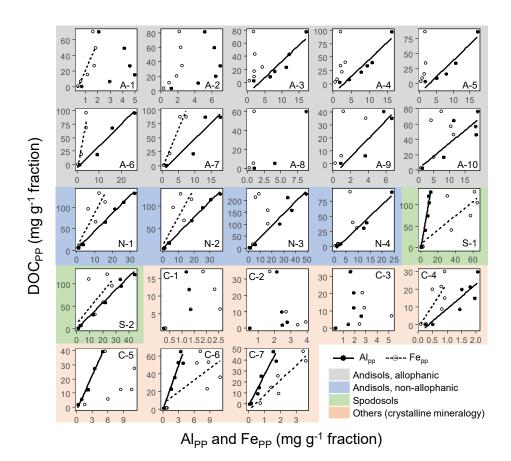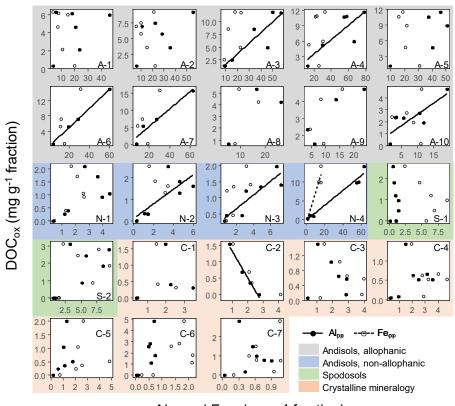
# Fig. A5



Figure. A5. Scattered plots of pyrophosphate-extractable Fe and Al against dissolved organic C concentration for each soil sample. Soil sample ID in each plot corresponds to that from Table 1. Solid lines represent significant linear regressions at $p < 0.1$.

# Fig. A6



Figure A6: Scattered plots of acid-oxalate-extractable Fe and Al against dissolved organic C concentration for each soil sample. Soil sample ID in each plot corresponds to that from Table 1. Solid lines represent significant linear regressions at p <0.1.
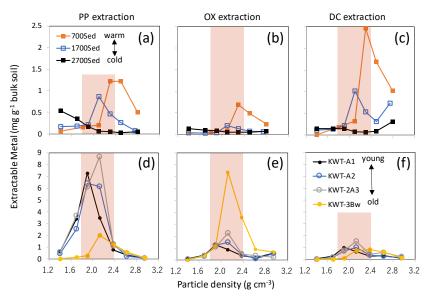
# Figure A7 and associated discussion



Figure A7. The distribution of the extractable metal phases (Al+0.5Fe) along the particle density gradient for two soil series. Upper three plots show PP- (a), OX- (b), and DC-extractable metals (c) for three A horizon soils under tropical forest along an elevation gradient from a weathered soil under warm climate at 700 m (sample ID: C5), moderately weathered soil at 1700 m (C6), and much less weathered soil at 2700 m (C7). The lower panels (d, e, f) showed surface and buried horizons of a non-allophanic Andisol profile (sample ID: N1-N4) that received multiple tephra deposits. Shaded zones show the meso-density range.

The relative balance of the three processes (OM supply and microbial processing, metal dissolution via weathering, and their binding/aggregation, Fig. 9) appear to control the nature of meso-density metal enrichment. Environmental gradients (e.g., climo- and chrono-sequences) give clear shifts in the balance of the three. Along a strong temperature gradient on a forested mountain slope, surface soils at higher altitudes experience slower rates of OM decay (thus higher OM accumulation) and mineral weathering than those at warmer lower-altitude soils. The majority of pedogenic metals in the 2700-m soil altitude (C-5) was present as PP-extractable phase and their distribution was peaked at <2.0 g cm$^{-3}$ fractions whereas the 700-m altitude soil (C-7) held the metals mostly as DC- and PP-extractable phases that were mainly present at >2.2 g cm$^{-3}$, and the mid-altitude soil (C-6) showed the patterns in between them (Fig. A7a-c). Meso-density metal enrichment was strongest in the 700-m soil. This result can be explained by (1) higher microbial processing of OM as the forest productivity and thus OM supply to soil was the highest (Kitayama and Aiba, 2002; Wagai et al., 2008), and (2) higher degree of weathering under the warm moist climate regime (Wagai et al., 2009).

Along with a volcanic soil profile experiencing up-building pedogenesis, we also observed the decline in metal$_{PP}$ and a concurrent increase in metal$_{OX}$ over pedogenic time (from upper to lower horizons), implying a shift in dominant metal phase from organo-metal complexes to short-range-order mineral. Concurrently, we found the increase in metal distribution from low towards higher density (Fig. A7d-f). The top three horizons (A1, A2, and 2A3) were developed over the last ca 10 kyr based on key tephra (Hijiori Pumice) identified between 2A3 and 3Bw horizon, suggesting that the organo-metallic glue enriched in PP-extractable phase was replaced by that rich in OX-extractable phase over ca 10 kyrs under reduced OM input (buried) condition.

These results therefore suggest general patterns in the localization of specific metal phases and the mode of OM-metal association across scales as follows: (i) Al and Fe released by weathering preferentially bind to organic ligands to form organo-metallic complex in OM-rich environment (e.g., surface horizon esp. under cooler climate) and (ii), under the pedogenic condition where net organic supply to mineral surface is limited for a prolonged time (e.g., rapid decomposition under warm, wet condition and deeper horizons), polymerization of Fe and Al (and Si) is facilitated. The latter leads to the formation of short-range-order mineral which is further transformed to well-crystalline oxides over time. In other words, pedogenic reactions such as dynamics of mobile weathering products and secondary mineral formation occurring at a pedon scale (e.g., the depth-dependent framework, (Lawrence et al., 2015)) can be observed within bulk soils by the current approach combining sequential density fractionation with the extraction of operationally-defined metal phases.

# Reference

Kitayama, K. and Aiba, S.I. (2002) Ecosystem structure and productivity of tropical rain forests along altitudinal gradients with contrasting soil phosphorus pools on Mount Kinabalu,Borneo. Journal of Ecology 90, 37.

Lawrence, C.R., Harden, J.W., Xu, X., Schulz, M.S. and Trumbore, S.E. (2015) Long-term controls on soil organic carbon with depth and time: A case study from the Cowlitz River Chronosequence, WA USA. Geoderma 247–248, 73-87.

Wagai, R., Mayer, L.M. and Kitayama, K. (2009) Extent and nature of organic coverage of soil mineral surfaces assessed by a gas sorption approach. Geoderma 149, 152-160.

Wagai, R., Mayer, L.M., Kitayarna, K. and Knicker, H. (2008) Climate and parent material controls on organic matter storage in surface soils: A three-pool, density-separation approach. Geoderma 147, 23-33.

Table A1. The results of qubic polynomical regression model applied to each of the four soil groups for pyrophosphate-extractable organic C ($DOC_{PP}$) and the sum of pyrophosphate- and oxalate-extractable C ($DOC_{PP}$+$DOC_{OX}$).

| | Allophanic Andisol | Non-allophanic Andisol | Spodic | Crystalline mineralogy |
|---|---|---|---|---|
| | $DOC_{PP}$ | | | |
| $r^2$ | 0.17 | 0.41 | 0.55 | 0.50 |
| RMSE | 0.12 | 0.24 | 0.12 | 0.11 |
| n | 49 | 27 | 14 | 39 |
| F | 3.13 | 5.21 | 4.05 | 11.86 |
| p | 0.0347 | 0.0068 | 0.040 | <0.0001 |
| | $DOC_{PP}$+$DOC_{OX}$ | | | |
| $r^2$ | 0.32 | 0.47 | 0.55 | 0.51 |
| RMSE | 0.12 | 0.22 | 0.12 | 0.11 |
| n | 49 | 27 | 14 | 39 |
| F | 6.99 | 6.73 | 4.12 | 12.27 |
| p | 0.0006 | 0.0020 | 0.0384 | <0.0001 |